Article

Current Biology

Functional Interactions between Newborn and Mature Neurons Leading to Integration into Established Neuronal Circuits

Graphical Abstract

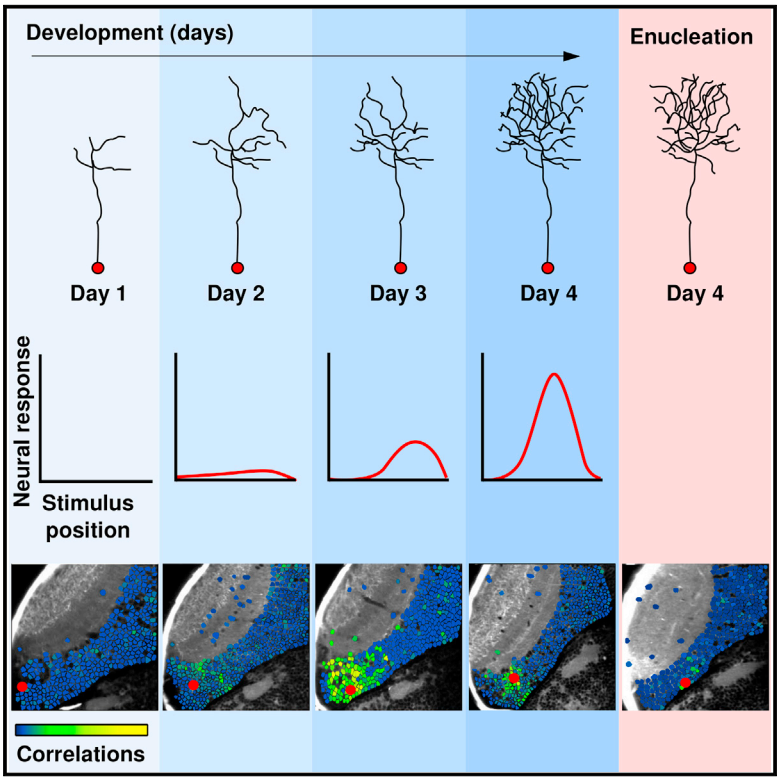

Authors

Jonathan Boulanger-Weill, Virginie Candat, Adrien Jouary, Sebastián A. Romano, Verónica Pérez-Schuster, Germán Sumbre

Correspondence

sumbre@biologie.ens.fr

In Brief

The functional interactions between newborn and mature neurons leading to the integration into established circuits during development remain unknown. Boulanger-Weill et al. describe this incorporation process and show that pre-synaptic visual inputs are required for the normal integration of newborn neurons into the mature tectal circuit.

Highlights

- Newborn neurons show simple morphology and intrinsic activity but no visual responses
- Then they show correlated spontaneous activity with functionally mature local neurons
- Finally, they acquire receptive fields and complex dendritic arbors
- Removal of retinal inputs prevents the incorporation process

Boulanger-Weill et al., 2017, Current Biology *27*, 1707–1720
June 19, 2017
http://dx.doi.org/10.1016/j.cub.2017.05.029

CellPress

Current Biology
Article

Functional Interactions between Newborn and Mature Neurons Leading to Integration into Established Neuronal Circuits

Jonathan Boulanger-Weill,[1] Virginie Candat,[1,5] Adrien Jouary,[1,5] Sebastián A. Romano,[1,2,5] Verónica Pérez-Schuster,[1,3,4] and Germán Sumbre[1,6,*]

[1]IBENS, Département de Biologie, Ecole Normale Supérieure, CNRS, Inserm, PSL Research University, 75005 Paris, France
[2]Instituto de Investigación en Biomedicina de Buenos Aires – CONICET – Partner Institute of the Max Planck Society, 1428 Buenos Aires, Argentina
[3]Laboratorio de Neurobiología de la Memoria, Departamento Fisiología, Biología Molecular y Celular, FCEyN, UBA and IFIBYNE-CONICET, Ciudad Universitaria, 1428 Buenos Aires, Argentina
[4]Departamento de Física, FCEyN, UBA and IFIBA-CONICET, Pabellón 1, Ciudad Universitaria, 1428 Buenos Aires, Argentina
[5]These authors contributed equally
[6]Lead Contact
*Correspondence: sumbre@biologie.ens.fr
http://dx.doi.org/10.1016/j.cub.2017.05.029

SUMMARY

From development up to adulthood, the vertebrate brain is continuously supplied with newborn neurons that integrate into established mature circuits. However, how this process is coordinated during development remains unclear. Using two-photon imaging, GCaMP5 transgenic zebrafish larvae, and sparse electroporation in the larva's optic tectum, we monitored spontaneous and induced activity of large neuronal populations containing newborn and functionally mature neurons. We observed that the maturation of newborn neurons is a 4-day process. Initially, newborn neurons showed undeveloped dendritic arbors, no neurotransmitter identity, and were unresponsive to visual stimulation, although they displayed spontaneous calcium transients. Later on, newborn-labeled neurons began to respond to visual stimuli but in a very variable manner. At the end of the maturation period, newborn-labeled neurons exhibited visual tuning curves (spatial receptive fields and direction selectivity) and spontaneous correlated activity with neighboring functionally mature neurons. At this developmental stage, newborn-labeled neurons presented complex dendritic arbors and neurotransmitter identity (excitatory or inhibitory). Removal of retinal inputs significantly perturbed the integration of newborn neurons into the functionally mature tectal network. Our results provide a comprehensive description of the maturation of newborn neurons during development and shed light on potential mechanisms underlying their integration into a functionally mature neuronal circuit.

INTRODUCTION

From embryonic development to adulthood, newborn neurons are continuously added to the vertebrate brain. This process is an important component of brain plasticity, permitting the formation of new memories [1] and adaptation of neural circuits to the ever-changing sensory environment [2]. Following differentiation, newborn neurons migrate from the zones of proliferation toward their final circuit targets, gain intrinsic excitability, acquire neurotransmitter identity, and develop dendritic arborizations [3]. Eventually, these recently born neurons receive synaptic inputs [4–6] and connect to post-synaptic partners [7, 8], indicating their integration into neuronal networks.

Studies of newborn neurons in the adult hippocampus dentate gyrus and the sub-ventricular zone have shed light on the sequence of events underlying their functional maturation [2, 4, 5, 9]. For instance, in the sub-ventricular zone, newborn neurons develop their functional properties during their migratory process. After arrival to the olfactory bulb, these neurons display spontaneous synaptic activity, suggesting their functional integration into functionally mature circuits [4]. The sensory properties of these neurons reach maturity following a brief period of enhanced sensory responsiveness [2]. Similarly, newborn granule cells in the hippocampus bypass inhibitory control, showing a transient increase in excitability and a broad tuning for afferent information [9, 10]. Despite these advances, the functional interactions between newborn and functionally mature neurons leading to the integration are poorly understood, and how this coordinated process occurs during development remains unknown.

Here, we addressed these open issues via a comprehensive in vivo approach in the visual system (optic tectum) of an intact, non-anesthetized, non-paralyzed developing vertebrate. We used two-photon microscopy, sparse electroporation, and transgenic zebrafish larvae expressing GCaMP5G. This approach enabled monitoring with single-cell resolution the development of the morphology and the induced and spontaneous activity of

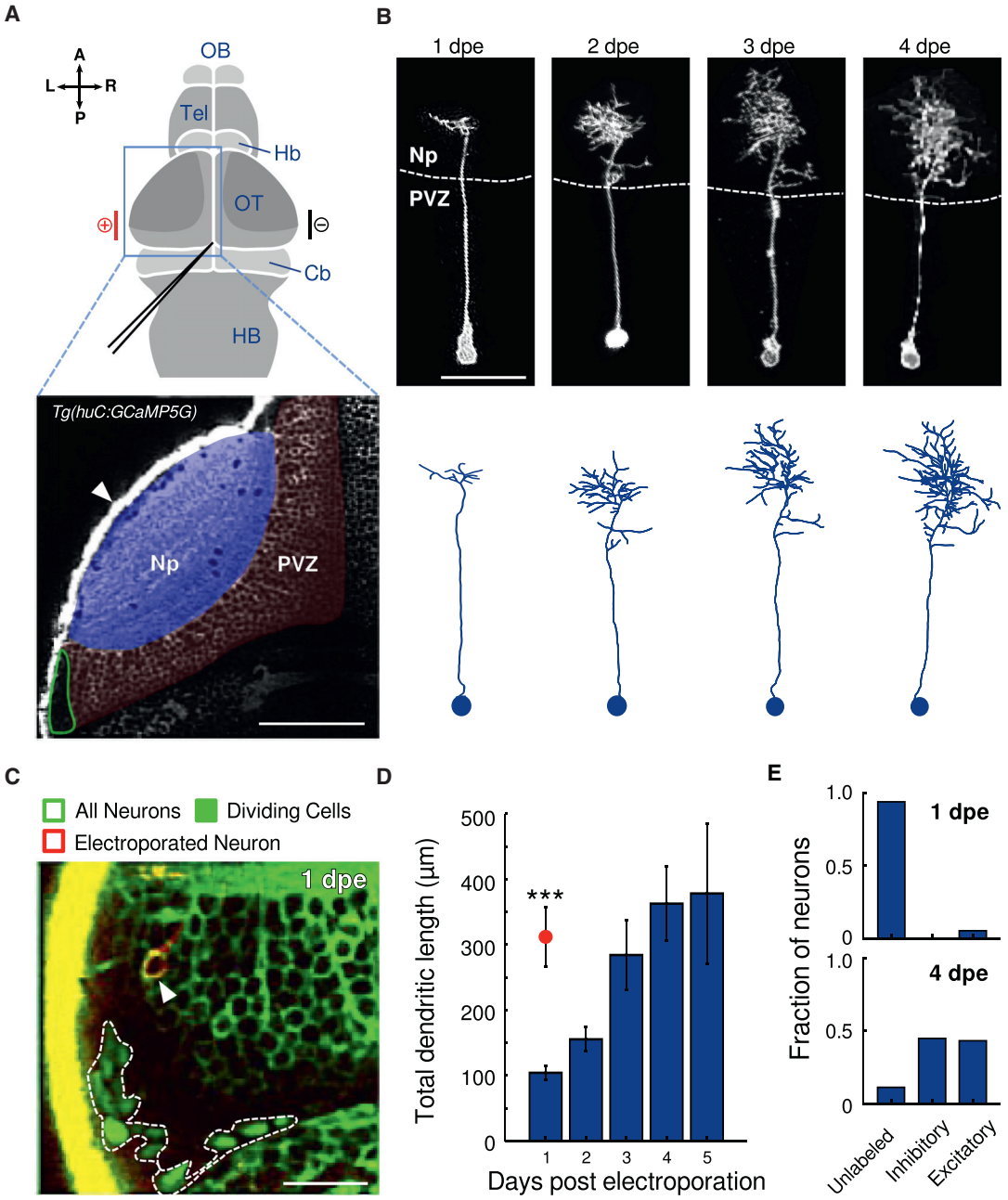

Figure 1. Morphological Development of Newborn Neurons and Emergence of Neurotransmitter Identity

(A) Top: schematic dorsal view of the zebrafish brain. The electroporated optic tectum (OT) is indicated by the blue square. The DNA injection capillary scheme is depicted in black. The electroporation electrodes are shown in red (cathode) and black (anode) bars. Cb, cerebellum; Hb, habenula; HB, hindbrain; OB, olfactory bulb; Tel, telencephalon. Bottom: Optical section of a *Tg(huC:GCaMP5G)* zebrafish larva showing pan-neuronal GCaMP5 expression corresponding to the area in the top scheme (blue rectangle). The periventricular zone (PVZ) of the OT left hemisphere is highlighted in red; Np, neuropil, highlighted in blue. The neurogenesis site is circled in green. The scale bar represents 50 μm. L, left; R, right; A, anterior; P, posterior.

(B) Example of a developing newborn-labeled neuron chronically imaged from 1 to 4 dpe. The neuron developed to become a non-stratified peri-ventricular neuron. Bottom: corresponding morphological reconstructions. The scale bar represents 20 μm.

(C) An optical section of the tectum's caudo-lateral region of an electroporated *Tg(EF1:mAG-hGem;huC:GCaMP5G)* larva (all neurons express GCaMP5G in the cytoplasm and dividing cells express the nuclear localized GFP mAG in the nucleus; dashed line). Note the non-fluorescence region between the dividing cells and the GCaMP5G-expressing neurons. This dark region corresponds to cells that exited the dividing cycle but are not yet neurons. An electroporated newborn neuron can be observed adjacent to the neurogenesis site (imaged at 1 dpe and expressing dTomatoCAAX; arrowhead). The scale bar represents 20 μm.

(D) Total dendritic length obtained from morphological reconstructions of newborn neurons from 1 to 5 dpe (n = 22, 17, 10, 12, and 3, respectively). Only one neuron was reconstructed per electroporated larva. The red circle represents the average dendritic length of functionally mature neurons at 1 dpe, n = 8. The error bars represent SEM. ***$p < 10^{-3}$.

(legend continued on next page)

newborn neurons from an early developmental stage to maturity. In addition, we compared the evolution of these parameters with respect to those of a large population of functionally mature neurons and computed their pairwise correlations to study the development of their functional interactions.

The optic tectum, homologous to the mammalian superior colliculus, is the zebrafish's most complex visual processing brain center. Despite the early developmental stage, the zebrafish larva is capable of performing complex tectum-dependent behaviors [11]. At 5 days post-fertilization (dpf), the tectal neurons are already tuned to visual stimuli of specific size, orientation, and direction [12–14] and zebrafish larvae are capable of performing complex tectum-dependent visuo-motor behaviors, such as prey capture [15]. In teleosts, the brain grows throughout the fish lifespan. Thus, newborn neurons are continuously added to functionally mature neuronal circuits from neurogenesis sites. In the optic tectum, the neurogenesis zone represents a cellular conveyor belt at the dorso-medial and caudo-lateral margins of the functionally mature circuit [16–18]. The neuroanatomy of the larva's optic tectum enables monitoring the morphology and dynamics of functionally mature networks and newborn neurons within the same optical plane. Thus, it is an ideal system to study the mechanisms underlying the incorporation of the newborn neurons into the functionally mature circuits.

In this study, we describe the development of newborn neurons in terms of their morphology, neurotransmitter identity, and spontaneous and visually evoked activity from an early immature to a functionally mature developmental stage. Although during the studied period the larva is still under development, the tectal circuit is already mature for its functional role (e.g., spatial detection of sensory stimuli and generation of the adequate motor behaviors). Moreover, tectal neurons already displayed stable dendritic arbors, neurotransmitter identity (excitatory or inhibitory), and different types of visual tuning curves and spatiotemporal patterns of spontaneous activity [12–14, 19–21]. At the onset of the expression of the electroporated plasmids, newborn neurons exhibited undeveloped dendritic arbors and no neurotransmitter identity. At this immature stage, they were unresponsive to visual stimulation but did show intrinsic spontaneous calcium transients. Later on, newborn neurons began to show spontaneous activity correlations with their functionally mature counterparts. Visually induced responses were very variable, displaying poor direction and orientation selectivity and unreliable receptive fields. By the end of the maturation process (4 days after being labeled), newborn-labeled neurons showed complex dendritic arbors and an established neurotransmitter identity (e.g., GABAergic or glutamatergic). At this stage, newborn-labeled neurons exhibited mature spatial receptive fields and robust spontaneous activity correlations with functionally mature neurons. Enucleations performed just before the electroporations significantly decreased the spontaneous correlations between newborn-labeled and functionally mature neurons, suggesting that pre-synaptic visual inputs are required for the normal integration of newborn neurons into the functionally mature tectal circuit.

RESULTS

Morphological Development of Newborn Neurons and Neurotransmitter Identity

To describe the morphological development of newborn neurons, we used an electroporation approach performed at 4 dpf [22] (plasmids: Tol2-*huC*:Gal4, Tol2-*2xUAS*:dTomato-CAAX, and *2xUAS*:Transposase; Figures 1A, S1A, and S1B; STAR Methods). This technique was innocuous to the larvae (Figure S1C) and capable of labeling single neurons (2.4 ± 0.26 cells per larva; n = 25 larvae; mean ± SEM). At 5 dpf (representing 1 day after electroporation [dpe]), when the optic tectum has already matured for its functional role (e.g., execution of prey capture behavior; Figure S1D), labeled neurons displayed small and undeveloped dendritic arbors (Figure 1B) compared to mature neuronal types at the same developmental stage (total dendritic length of immature neurons at 5 dpf: 104 ± 11 μm; mature neurons at 5 dpf: 312 ± 43 μm; $p = 1.6 \times 10^{-4}$; Mann-Whitney U test; Figures 1D and S1E; STAR Methods). These immature neurons were generally located in a caudo-lateral region of the optic tectum, adjacent to dividing neuronal progenitors (Figure 1C). Morphological reconstruction of the labeled neurons from 1 to 4 dpe (corresponding to 5–8 dpf; Figure 1B) showed an ~4-fold increase in their total dendritic length (from 104 ± 11 to 363 ± 44 μm). The latter was reminiscent of the dendritic length of mature neurons [23] (Figure 1D).

Previous studies suggest that the majority of the tectal neurons are either glutamatergic or GABAergic with few cholinergic neurons [24]. To investigate the development of the neurotransmitter identity of the labeled newborn neurons, we electroporated Tol2-*huC*:Gal4 and Tol2-*10xUAS*:mTagBFP2CAAX plasmids (Figure S1B) in transgenic zebrafish larvae expressing GFP under the gad1b promoter and DsRed under the vglut2a promoter (*Tg(gad1b:GFP;vglut2a:loxP-DsRed-loxP-GFP)*). At 1 dpe, the large majority of the labeled newborn neurons were negative for *gad1b*:GFP and *vglut2a*:DsRed (94%; n = 34 neurons from 13 larvae; Figures 1E and S1F). In contrast, at 4 dpe, 87% (n = 62 neurons from 29 larvae) of the labeled newborn neurons were already positive for *gad1b*:GFP or *vglut2a*:DsRed (45% and 42%, respectively).

In the zebrafish larva optic tectum, several morphological classes of neurons have been identified [25] with some associated with neuronal functional properties, such as direction or size selectivity [12, 26]. The electroporation approach labeled a variety of tectal cell types of the periventricular layer (non-stratified neurons, bi-stratified neurons, and projection neurons; 47.8%, 30.4%, and 21.7%, respectively; n = 23 neurons at 4 dpe from 23 larvae; Figure S1G). Whether this ratio is representative of the functionally mature tectal population remains to be studied.

(E) Fraction of excitatory and inhibitory newborn-labeled neurons in *Tg(gad1b:GFP;vglut2a:loxP-DsRed-loxP-GFP)* larvae at 1 and 4 dpe. For visualization of the newborn-labeled neurons, a blue fluorescence protein was used for the electroporations (1 dpe: n = 34 neurons from 13 larvae; 4 dpe: n = 62 neurons from 29 larva).

See also Figure S1.

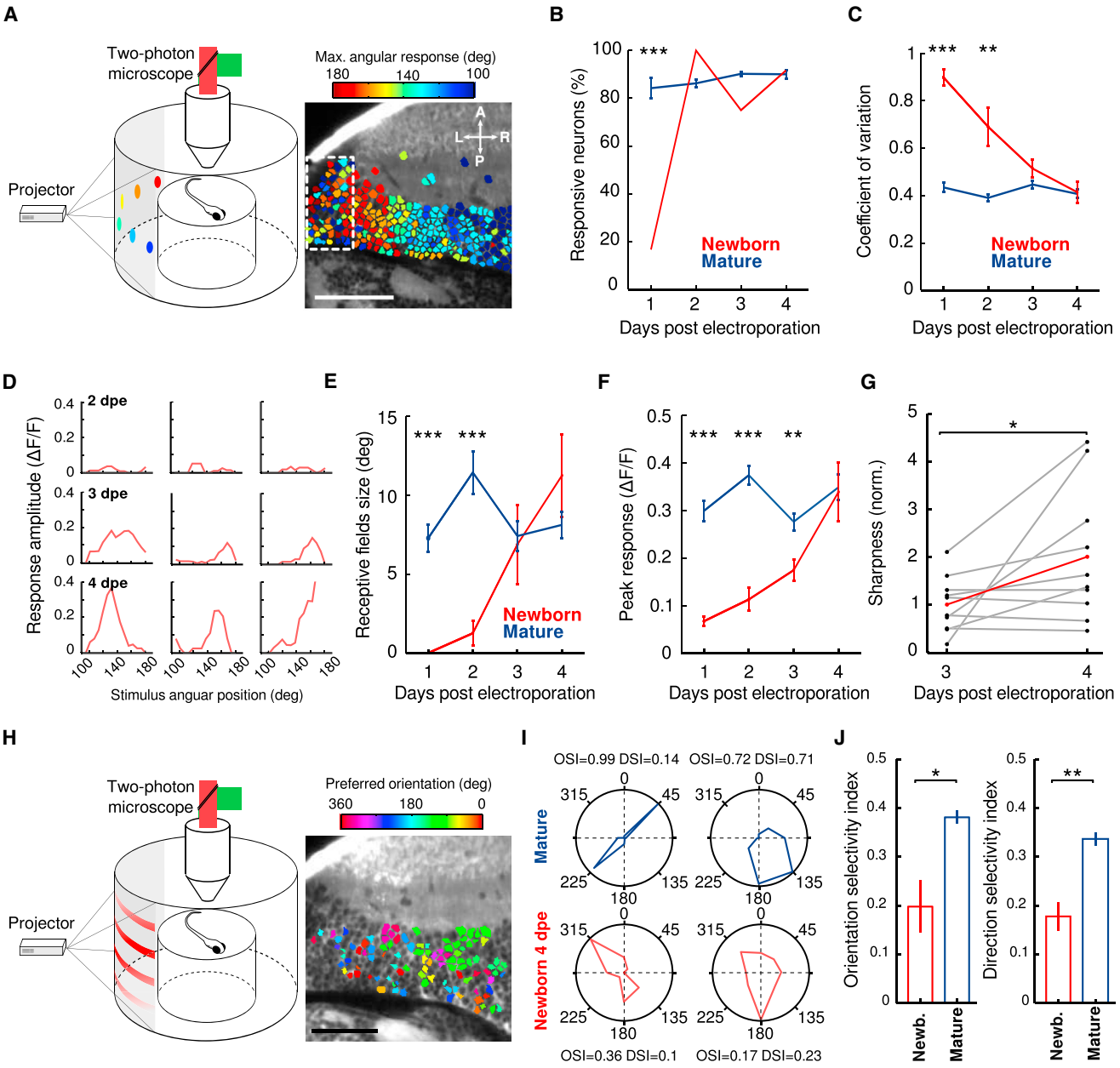

Figure 2. Development of Visually Induced Properties of Newborn-Labeled Neurons

(A) Schematic drawing of the recording chamber and the visual stimuli presented to study the visual receptive field of tectal neurons. Examples of light spot stimuli projected on a screen covering a large portion of the larva's field of view are shown. The light spots are color coded according to their angular position. Right: example of an optical section of the optic tectum showing the functional retinotopic map (note the graded change in colors along the rostro-caudal axis. The neurons are color-coded according to the peak of the neurons' receptive field. Dashed region indicates the region neighboring the neurogenesis site, containing neurons with weak visual receptive fields and lacking retinotopy organization. Arrows indicate the orientation of the larva: L, left; R, right; A, anterior; P, posterior. The scale bar represents 50 μm.

(B) Percentage of visually responsive neurons during development both for newborn (red) and the whole neuronal population (blue) from 1 to 4 dpe (n = 6, 6, 12, and 12 newborn developing neurons and n = 1,883, 2,240, 4,752, and 3,454 neurons from 5, 6, 13, and 10 larvae, respectively). The error bars represent SEM. ***$p < 0.001$.

(C) Developmental dynamics of response variability to light spots, quantified as the coefficient of variation, for newborn (blue) and the whole neuronal population (red). The error bars represent SEM. ***$p < 0.001$; **$p < 0.01$.

(D) Three examples of visual receptive fields (the amplitude of the Ca^{2+} response with respect to the angular position of the presented light spot within the larva's field of view), recorded at 2, 3, and 4 dpe. Note the emergence of the receptive fields at 3 dpe.

(E and F) Development of the size (E) and peak amplitude (F) of the receptive fields of newborn (red) and whole neuronal population (blue) from 1 to 4 dpe (n = 8 newborn-labeled neurons for each developmental stage and n = 1,565, 2,379, 1,680, and 1,841 functionally mature neurons from 9, 10, 9, and 10 larvae, respectively). The error bars represent SEM. ***$p < 0.001$; **$p < 0.01$.

(legend continued on next page)

Development of Visually Induced Properties of Newborn Neurons

To study the development of the functional properties of the newborn neurons, we used two-photon microscopy in combination with zebrafish larvae pan-neuronally expressing the genetically encoded Ca^{2+} indicator GCaMP5, *Tg(huC:GCaMP5G).*

Tectal neurons in the zebrafish larva have two well-studied functional properties: visual receptive fields and direction and orientation selectivity [13, 14, 26]. To characterize the visual receptive fields of newborn neurons, we presented to the larvae 5° light spots at different positions in their field of view. To compute their direction and orientation selectivity, we used moving grids of different orientations. We characterized these functional properties throughout the maturation of the newborn neurons, from 1 to 4 dpe (Figure 2A). At 1 dpe, just a small fraction (16.6%; n = 6 newborn neurons from five larvae; Figure 2B) of the electroporated population was responsive versus 84.5% ± 4.2% among the functionally mature population (n = 1,883 neurons from five larvae; Figure 2B; see STAR Methods for the definition and determination of functionally mature neurons). In contrast, at 2 dpe, the percentage of responsive newborn neurons to visual stimuli was already similar to that of functionally mature neurons. This fraction remained relatively stable thereafter (from 2 to 4 dpe; newborn neurons: 100%, 75%, and 91.7%; functionally mature neurons: 86.3% ± 1.6%, 90.2% ± 1.0%, and 90.0% ± 1.7%; Figure 2B). Although newborn neurons began to show visually induced responses at an early stage of their development, their responses were very variable (coefficient of variation [CV] at 1 or 2 dpe: 0.90 ± 0.04 and 0.69 ± 0.09, respectively; n = 8 electroporated neurons at each stage; Figure 2C; STAR Methods). This variability gradually decreased, reaching similar values to those of functionally mature neurons (at 3 dpe, n = 8 newborn neurons: 0.51 ± 0.04, n = 1,680 functionally mature neurons: 0.45 ± 0.02, p = 0.06, from nine larvae; at 4 dpe, n = 8 newborn neurons: 0.41 ± 0.04, n = 1,841 functionally mature neurons: 0.41 ± 0.02, p = 0.83, from ten larvae; Mann-Whitney U test; Figure 2C).

The optic tectum contains neurons with distinctive visual receptive fields. At the network level, these neurons are organized along the tectum caudo-rostral axis, forming a functional retinotopic map [14, 21]. We therefore studied the development of the visual receptive fields in newborn neurons and compared them to those of the functionally mature population (Figure 2D). To that end, we quantified the size, peak amplitude, and sharpness of the receptive fields from 1 to 4 dpe. We found that, at 1 or 2 dpe, the receptive fields were not spatially tuned for a specific position in the field of view (Figures 2C–2E). As the newborn neurons developed, the size of the receptive fields gradually increased, reaching values similar to those of functionally mature neurons between 3 and 4 dpe (at 3 dpe, newborn neurons: 6.9 ± 2.7, n = 8 newborn neurons, functionally mature neurons: 7.4 ± 1.0, n = 1,680, p = 0.52, from eight larvae; at 4 dpe, newborn neurons: 11.2 ± 2.8, n = 8, functionally mature neurons: 8.1 ± 0.9, n = 1,841, p = 0.35, from eight larvae; Mann-Whitney U test; Figure 2E). The amplitude of the peak response followed similar developmental dynamics, reaching values similar to those of functionally mature neurons at 4 dpe (newborn neurons: 0.34 ± 0.07; functionally mature neurons: 0.35 ± 0.03; p = 0.70; Mann-Whitney U test; Figure 2F). Sharpness of the receptive fields was quantified for tuned and reliable receptive fields (from 3 to 4 dpe) and significantly increased from 3 to 4 dpe, reaching similar values to those of the functionally mature neuronal population (1.00 ± 0.18 to 2.00 ± 0.44, respectively, n = 10 chronically monitored newborn neurons from ten larvae, p = 0.044, one-tailed Wilcoxon rank sum test; functionally mature population: 2.03 ± 0.16, p = 0.38 with newborn-labeled neurons at 4 dpe, Mann-Whitney U test; Figure 2G).

Several tectal neurons are also selective to the direction and/or the orientation of moving visual stimuli [14, 21, 26–28]. To determine the orientation and the direction selectivity of the newborn-labeled neurons and the functionally mature neuronal population, we presented to the larvae gratings moving in eight different directions (Figures 2H–2J). As observed for the 5° light spots, the response variability of the 1-dpe newborn neurons was significantly larger than the functionally mature ones (newborn neurons' CV: 0.93 ± 0.0, n = 7; functionally mature neurons' CV: 0.28 ± 0.02, n = 973; p = 0.008; from five larvae; Mann-Whitney U test; Figure S2A). Along the same lines, the topography of the response variability of tectal neurons showed high coefficient of variation values (Figure S2B) and weak responsiveness (Figures S2C and S2D) in the proximity of the neurogenesis site. As newborn neurons developed, the response variability to moving gratings gradually decreased, reaching similar values to those of the functionally mature neurons at 3 or 4 dpe (at 3 dpe, newborn neurons: 0.38 ± 0.06, n = 6, functionally mature neurons: 0.31 ± 0.02, p = 0.29, n = 858, from four larvae; at 4 dpe: newborn neurons: 0.35 ± 0.14, n = 3, functionally mature neurons: 0.32 ± 0.04, n = 453, p > 0.5, from two larvae; Mann-Whitney U test; Figure S2A). Despite this decrease in the variability of the response, their orientation and direction selectivity of the newborn-labeled neurons remained significantly smaller than those of the functionally mature neuronal population (3 and 4 dpe; n = 9 newborn neurons, DSI: 0.18 ± 0.03, OSI: 0.20 ± 0.05; n = 1,311 functionally mature neurons, DSI: 0.34 ± 0.01,

(G) Normalized sharpness of the same newborn-labeled neurons imaged at 3 and 4 dpe. Data are normalized to the average value of newborn-labeled neurons at 1 dpe. The red line indicates the average sharpness. *p < 0.05.

(H) Schematic drawing of the recording chamber and the visual stimuli presented to study the direction and orientation selectivity of tectal neurons. Example of a moving grating projected on a screen covering a large portion of the larva's field of view. Right: example of an optical section of the optic tectum showing the preferred orientation angle for the direction-selective neurons (direction selectivity index [DSI] > 0.3). Neurons with DSI ≤ 0.3 were not labeled. The scale bar represents 50 μm.

(I) Examples of the direction and orientation selectivity (polar plots) of two mature (blue) and two 4-dpe newborn-labeled (red) neurons. The corresponding direction and orientation selectivity indexes (DSI and OSI) are shown above and below the polar graphs.

(J) Average of the orientation (left) and direction selectivity (right) indexes for 3- to 4-dpe newborn-labeled (red) and functionally mature (blue) neurons. *p < 0.05; **p < 0.01. The error bars represent SEM.

See also Figure S2.

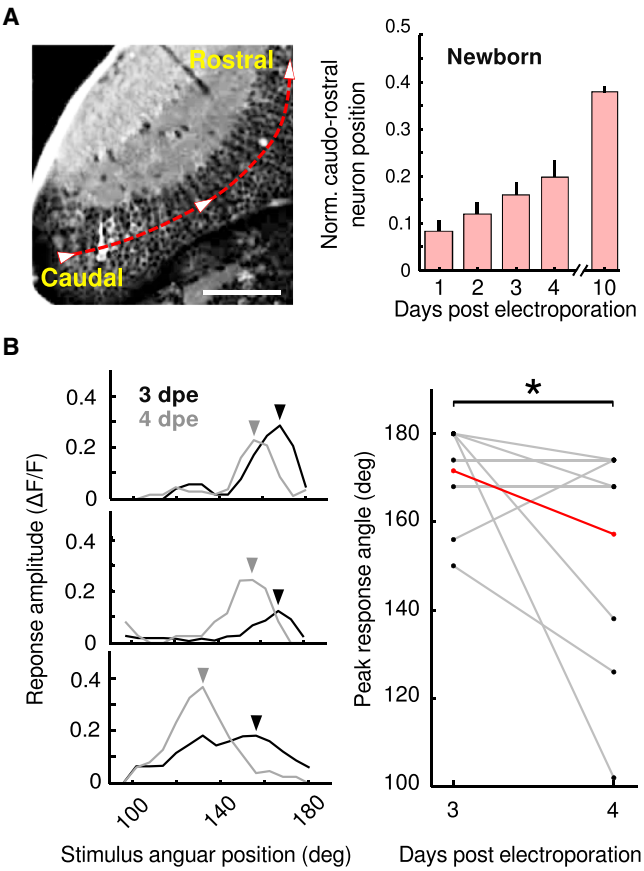

Figure 3. Newborn Neurons Shift the Peak's Position of Their Receptive Fields as They Develop

(A) Left: optical section of the optic tectum of a *Tg(huC:GCaMP5G) larva* showing the caudo-rostral axis (red). This axis was used for normalization of the position of neurons across recordings. The scale bar represents 50 μm. Right: the average of the normalized caudo-rostral position of newborn-labeled neurons, from 1 to 4 and 10 dpe. Note the gradual displacement of the neurons away from the neurogenesis region. The error bars represent SEM.

(B) Left: three examples of the spatial tuning curves of chronically recorded newborn-labeled neurons at 3 (black) and 4 (gray) dpe. Note the displacement of peaks of the tuning curves between 3 and 4 dpe (arrowheads). The displacement is always toward more rostral positions. Right: the angle of the stimulus that generated the strongest responses (peak) at 3 and 4 dpe. Gray lines connect the same newborn-labeled neuron imaged at 3 and 4 dpe. The red line indicates the average of the stimulus' angle that induced the peak response. *$p < 0.05$.

OSI: 0.38 ± 0.01; p = 0.001 and p = 0.037, respectively, from six larvae; one-tailed Wilcoxon rank sum test; Figures 2I and 2J). Taken together, our observations suggest that newborn neurons acquire robust and sharply tuned receptive fields within 2 or 3 days after the emergence of retinal connectivity, while being less tuned to orientation or direction of motion. Although the newborn-labeled neurons developed into several morphological classes (Figure S1G) and neurotransmitter identities (Figure 1E), it is possible that a specific class of highly direction-selective neurons cannot be labeled using approach. Alternatively, it is possible that high direction or orientation indexes emerge beyond 4 dpe.

Newborn Neurons Shift the Peaks of Their Receptive Fields as They Develop

Previous observations have demonstrated that connections arising from the retina continuously shift toward more caudal regions of the tectum to maintain retinotopy despite the addition of newborn tectal neurons [29, 30]. At least for the imaged optical planes, we observed that newborn neurons gradually moved away from the neurogenic zone along the caudo-rostral axis of the optic tectum (normalized coordinates from 1, 2, 3, 4, and 10 dpe: 0.08 ± 0.02, 0.12 ± 0.02, 0.16 ± 0.02, 0.20 ± 0.03, and 0.38 ± 0.01; n = 6, 15, 21, 15, and 3 newborn-labeled neurons from 6, 10, 17, 11, and 2 larvae; Figure 3A). This observation supports the previously proposed hypothesis that tectal neurons are passively displaced by the addition of newborn neurons at the dividing caudal neurogenic neuroepithelium [16, 18].

In accordance with this displacement, we observed a significant shift of the peak of the visual receptive fields from 3 to 4 dpe (Figure 3B, left panel). This shift matched the expected direction with respect to the physical displacement of the neurons along the caudo-rostral axis: older neurons had spatial tuning curves peaking at more rostral positions in the field of view (smaller angles) than younger neurons (3 dpe neurons: 172.0° ± 3.37°; 4 dpe neurons: 155.2° ± 7.91°; n = 10 newborn-labeled neurons from ten larvae; p = 0.017; one-tailed Wilcoxon rank sum test; Figure 3B, right panel). This result suggests that, despite the continuous addition of newborn neurons to the optic tectum, retinotopy is conserved by a progressive shift of the spatial tuning curves as the neurons get older.

Spontaneous Activity Correlations between Newborn and the Functionally Mature Neuronal Population

Sensory brain areas are continuously active, even in the absence of external stimulation. This ongoing spontaneous activity in sensory brain areas has complex spatiotemporal patterns, in some cases representing relevant sensory maps [21, 31, 32], and reflects the functional connectivity of neuronal circuits [33]. Therefore, to study the development of the functional interaction dynamics between newborn neurons and their functionally mature counterparts, we monitored spontaneous activity of newborn neurons and the functionally mature tectal circuit at four consecutive developmental stages (from 1 to 4 dpe; newborn neurons = 6, 15, 21, and 15 neurons from 6, 10, 17, and 11 larvae; 401.8 ± 12.6 total neurons per larva from 44 larvae; Figure 4).

The labeled newborn neurons already exhibited spontaneous Ca^{2+} activity at 1 dpe (Figure 4; Table S1). We examined the development of the Pearson's pairwise correlations between the Ca^{2+} dynamics of the newborn neurons and the large functionally mature neuronal population from 1 to 4 dpe (Figure 5A). For each dataset, significant correlations were calculated using surrogate shuffled datasets (Figure 5B; STAR Methods). We observed that at 1 dpe, the mean of the significant correlations between newborn and functionally mature neurons was very low and significantly different from the mean correlation values between functionally mature tectal neurons (0.06 ± 0.003 for newborn neurons; 0.13 ± 0.01 for functionally mature neurons; p = 0.004; Mann-Whitney U test; Figure 5D). At 2 dpe, the average correlation values between newborn and functionally mature neurons increased gradually, reaching those found

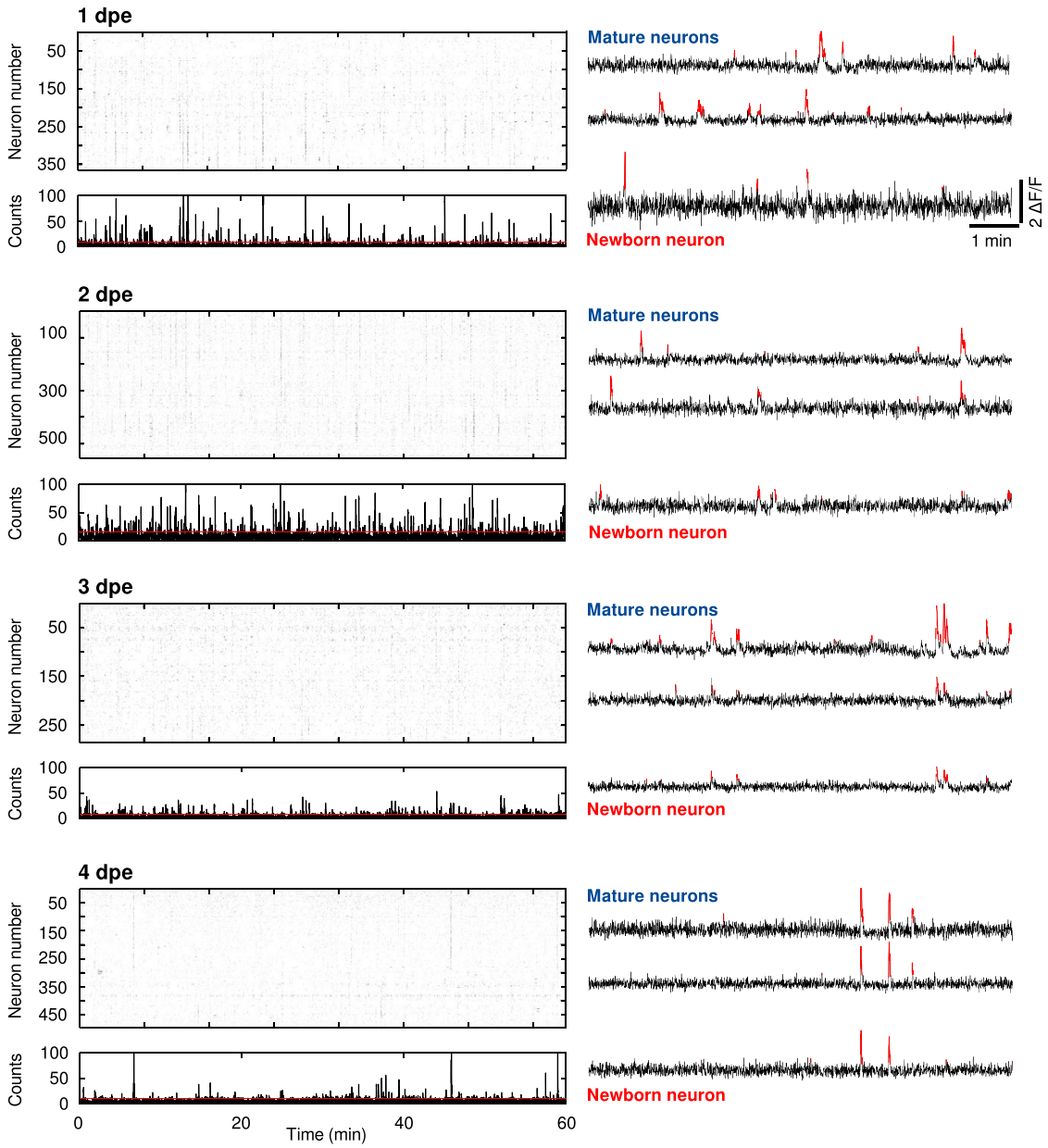

Figure 4. Spontaneous Activity of the Optic Tectum at Different Developmental Stages

Left: raster plot examples of significant spontaneous Ca^{2+} transients, revealing episodes of synchronous activations at 1–4 dpe (5–8 dpf). Bottom: histogram of the rasters above. The red line indicates the threshold for significant population events. Right: representative traces of mature (top two traces) and newborn neurons (bottom trace). Significant ΔF/F transients are highlighted in red.

See also Table S1.

among the functionally mature neuronal population at 3 dpe (at 2 dpe, 0.10 ± 0.02 for newborn neurons, 0.15 ± 0.02 for functionally mature neurons, p = 0.035; at 3 dpe, 0.11 ± 0.01 for newborn neurons, 0.11 ± 0.01 for functionally mature neurons, p = 0.26; Mann-Whitney U test; Figure 5D).

To learn about the spatial structure of the significant correlations (representing the topography of the functionally connected neurons), we computed the relationship between the percentage of significant correlations and the physical distance between the newborn and the functionally mature tectal neurons. We observed that functionally mature neurons showed a strong bias for correlations at short distances (from 1 to 4 dpe: 61.5% ± 6.3%; 54.7% ± 5.4%; 45.2% ± 4.7%; and 40.8% ± 7.4% of correlations were significant within an ~20-μm radius from each functionally mature neuron), which remained relatively stable during the 4 consecutive days (Figures 5C and S3B, blue curves). At 1 dpe, newborn neurons displayed a very low percentage and average of significant correlations with the functionally mature tectal neurons (0.45% ± 0.1% of the correlations were significant; Figures 5C and S3B, red curves). At 2 dpe,

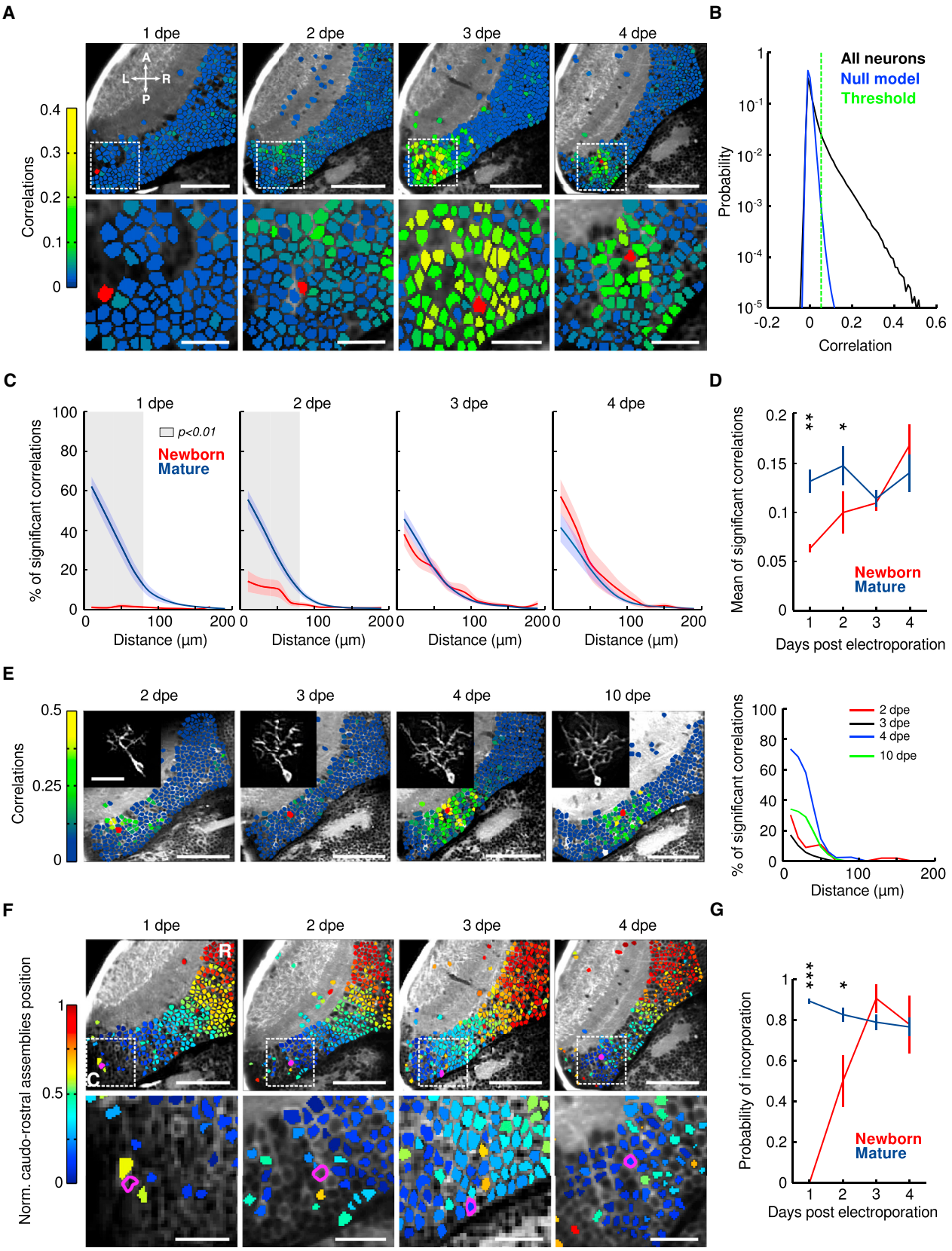

(legend on next page)

the percentage and average of significant correlations increased, mainly at short distances (12.40% ± 3.67% the correlations were significant within 40 μm of newborn neurons; Figures 5C and S3B). By 3 dpe, the spatial distribution of significant correlations and the average values of these correlations were not significantly different from those observed among functionally mature neurons. No further significant increase of these measurements were observed at 4 dpe (Figures 5A–5D and S3B).

These results were obtained by monitoring different newborn neurons at the different developmental stages. Yet, in a few cases, we were able to image and analyze chronically the same newborn neuron for several consecutive days. These chronic experiments showed similar developmental dynamics as those observed when analyzing different neurons at each developmental stage (see Figures 5E and S3A for examples). Although the developmental dynamics of newborn neurons were quantified for 4 consecutive days for the majority of cases, in a few instances, we succeeded in monitoring the spontaneous activity dynamics for up to 10 days (Figure 5E). Although at 10 dpe the monitored neurons showed slightly weaker correlations, they still displayed complex dendritic arbors, strong pairwise correlations with surrounding neurons, and a spatial distribution of the correlations reminiscent of those observed at 4 dpe (Figure 5E). The weaker correlations could reflect a refinement of the functional connectivity of the newborn-labeled neurons (Figure 5E, right panel, green curve). Alternatively, they could also indicate the emergence of new extra-tectal afferents that may alter the intra-tectal correlations. Nevertheless, the existence of significant correlations at 10 dpe demonstrates that the functional incorporation of newborn neurons into functionally mature circuits is a long-lasting process underlying the continuous growth of the tectal circuit.

In the zebrafish optic tectum, the spontaneous activity is organized in distinct topographically compact neuronal assemblies grouping neurons with similar visual receptive fields. These functional assemblies are tuned to behaviorally relevant features (e.g., the size of a prey), and in some cases, their activity is predictive of tail movements [21]. Therefore, we tested the probability of a newborn neuron of belonging to one of the functionally mature functional assemblies of the optic tectum (Figure S3C). We observed that, at 1 dpe, newborn neurons did not belong to any of these neuronal assemblies. The probability of belonging increased at 2 dpe and became similar to that of functionally mature neurons at 3 or 4 dpe (Figures 5F and 5G; $p < 0.001$; $p = 0.023$, 0.12, and 0.94, respectively; Mann-Whitney U test). A similar phenomenon was observed when calculating the average maximal principal component (PC) loadings of the newborn-labeled and functionally mature neurons (no threshold was used for defining the assemblies; Figure S3D; STAR Methods).

Furthermore, analysis of the level of significant correlations (X^2 distance; Figure S3E; STAR Methods) across all tectal neurons within a single optical plane showed a distinctive group of neurons with significantly lower correlation coefficients with respect to the rest of the tectal population. These uncorrelated neurons were located in a spatially constrained tectal area corresponding to that populated by the labeled newborn neurons at 1 dpe (Figures 1A and 1C). Despite their low level of pairwise correlations with the rest of the network, these neurons showed spontaneous Ca^{2+} events with frequencies and amplitudes similar to those of the rest of the tectal population (Figures S3F and S3G). These results suggest that the progressive increase in the pairwise correlations is not due to an increase in the amplitude and frequency of spontaneous calcium events during the development of newborn neurons but rather to their functional connectivity. Overall, these experiments show that newborn neurons functionally connect with the surrounding functionally mature tectal neurons after becoming responsive to visual stimulation (Figure 5A).

Figure 5. Spontaneous Activity Correlations between Newborn and Functionally Mature Tectal Neurons

(A) Top: examples of optical planes of the optic tectum at 1–4 dpe (5–8 dpf). Neurons are color coded according to their pairwise correlation values (color scale bar) with the newborn neuron (red neuron). The scale bars represent 50 μm. Bottom: zoomed image of the dashed areas on top. The scale bars represent 20 μm. Neurons involving few pixels (less than five) or with unstable baselines (rapid changes generally indicating movement artifacts) were left unlabeled. L, left; R, right; A, anterior; P, posterior.

(B) Probability density for the correlations between the newborn-labeled and the functionally mature neurons. Black, the pairwise correlations; blue, the corresponding null model. The null model was used to determine significant correlations (threshold: $p < 0.01$; dashed green line).

(C) The developmental dynamics of the relationship between the percentage of significant correlations and the physical distance between the neurons for the newborn-labeled neurons (red) and the functionally mature neurons (blue) from 1 to 4 dpe. Confidence intervals show SEM. Gray shaded areas indicate significant differences between newborn and functionally mature curves ($p < 0.01$; Mann-Whitney U test).

(D) The developmental dynamics of the average of the significant correlations between newborn-labeled neurons and the rest of the tectal neurons (red) and the significant correlations between the functionally mature neurons (blue). *$p < 0.05$; **$p < 0.01$. The error bars represent SEM.

(E) Left: example of the same newborn-labeled neuron chronically imaged at 2, 3, 4, and 10 dpe. Tectal neurons are color coded according to their pairwise correlation values with the newborn-labeled neuron (red). The scale bars represent 50 μm. Note their displacement away from the unlabeled neurogenesis region. Insets represent the morphology of the labeled neuron. The scale bar represents 20 μm. Right: relationship between the significant correlations between the newborn-labeled neuron with the rest of the imaged tectal neurons and the physical distance between the neurons for each imaged developmental stage (2, 3, 4, and 10 dpe).

(F) Top: developmental dynamics of the incorporation of newborn-labeled neurons into neuronal tectal assemblies. The tectal neurons are color coded according to the assembly they belong to (the position of the assembly along the caudo-rostral tectal axis). The newborn-labeled neuron is colored in magenta. The scale bars represent 50 μm. Bottom: zoom of the dashed areas in the top panel. The newborn-labeled neuron is circled in magenta. Note that, only at 3 dpe, the newborn-labeled neuron is also colored in blue, indicating that it is part of one of the assemblies. Neurons involving few pixels (less than five) or with unstable baselines (rapid changes generally indicating movement artifacts) were left unlabeled. The scale bars represent 20 μm.

(G) Probability of incorporation of newborn-labeled neurons into the neuronal assemblies (red) and the probability of the functionally mature neurons to belong to one of the neuronal assemblies (blue) for 1–4 dpe (newborn neurons: n = 6, 15, 21, and 15; functionally mature neurons: n = 1,962, 3,564, 5,296, and 3,969 from 6, 10, 17, and 11 larvae, respectively). *$p < 0.05$; ***$p < 0.001$. The error bars represent SEM.

See also Figure S3.

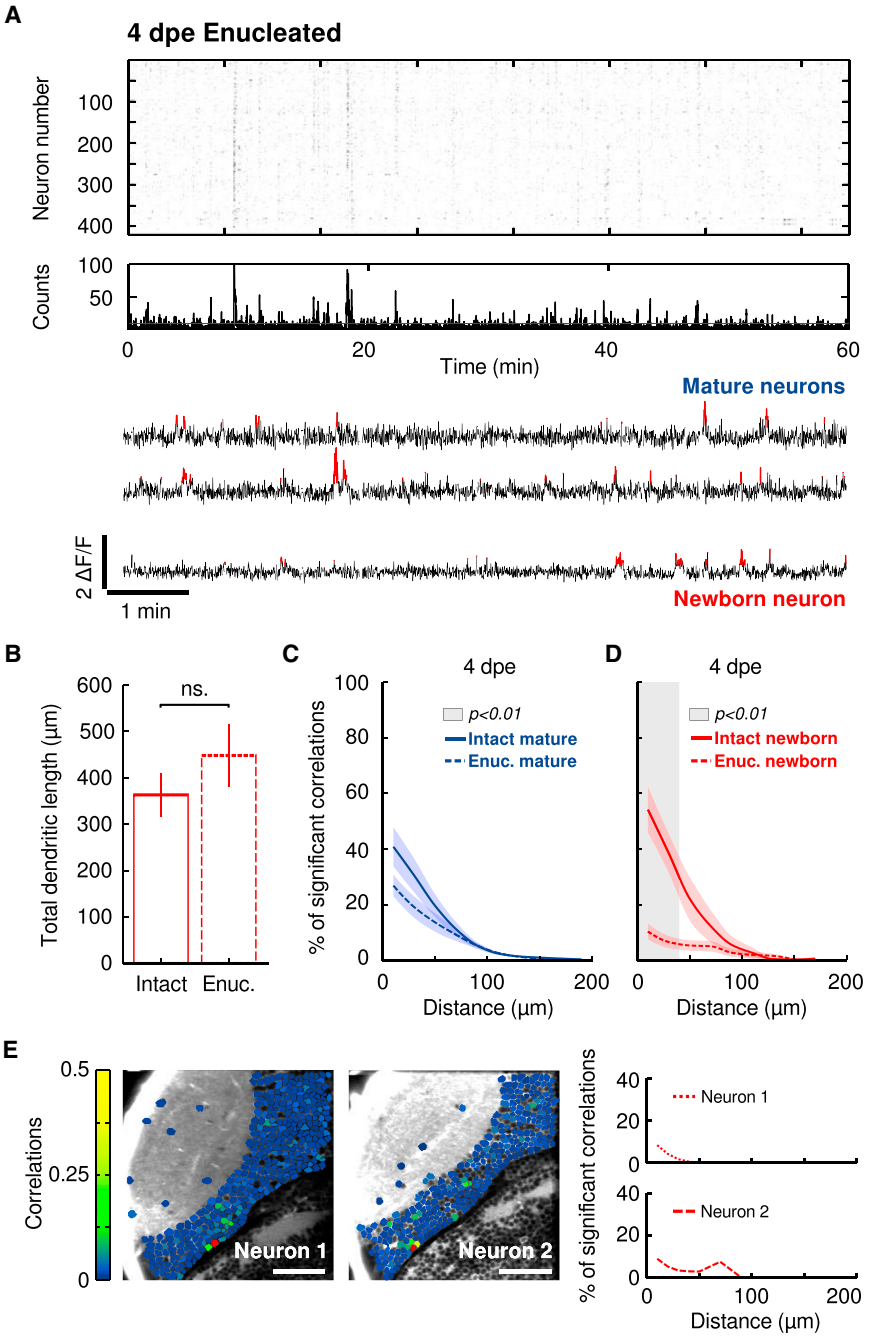

Figure 6. Retinal Inputs Are Necessary for the Proper Integration of Newborn Neurons into Functionally Mature Sub-circuits

(A) Top: Representative raster plot of significant spontaneous Ca^{2+} transients, revealing episodes of synchronous activations at 4 dpe (8 dpf) in enucleated conditions. Middle: histogram of the raster. The red line indicates the threshold for significant population events. Bottom: representative traces of mature (top traces) and newborn neurons (bottom trace). Significant ΔF/F transients are highlighted in red.

(B) Average of the total dendritic length of newborn-labeled neurons in intact (solid box) and enucleated (dashed box) 4-dpe larvae. ns, non-significant. The error bars represent SEM.

(C) The relationship between the percentage of significant correlations among functionally mature neurons in enucleated (dashed line) and intact (solid line) larvae and the physical distance between the neurons. Note that the two curves are not significantly different.

(D) The same as (C), but for the correlations between newborn-labeled neurons and the rest of the tectal neurons. Note the significant difference between the two curves for short distances. The gray shaded area indicates the significant difference between the curves ($p < 0.01$; Mann-Whitney U test). Confidence intervals show the SEM.

(E) Two examples of the pairwise correlations between newborn-labeled and the rest of the tectal neurons at 4 dpe. Left: optical sections of the optic tectum with neurons color coded (color scale bar) according to their pairwise correlations with the newborn-labeled neuron (red). Right: the relationship between the percentage of significant correlations between the newborn-labeled neuron and the rest of the tectal neurons and the physical distance between them for the two examples on the left. Note the inability of the newborn-labeled neurons to incorporate into the tectal circuit in enucleated larvae. Neurons involving few pixels (less than five) or with unstable baselines (rapid changes generally indicating movement artifacts) were left unlabeled.

See also Figure S4 and Table S1.

Retinal Inputs Are Necessary for the Proper Integration of Newborn Neurons into Functionally Mature Sub-circuits

To study the mechanisms underlying the incorporation of newborn neurons into functionally mature sub-circuits, we performed, just before the electroporation (~3.5 dpf), unilateral enucleations of the contralateral eye to the monitored tectal hemisphere (in the zebrafish larva, the retina projects exclusively to the contralateral hemisphere; see STAR Methods). This procedure chronically deprived the optic tectum of all retinal afferents before the labeled newborn neurons became responsive to visual stimuli. Under these conditions, the functionally mature population developed under normal retinal conditions (before the enucleations), whereas the newborn neurons developed under retinal deprivation (in the absence of visual stimuli or spontaneous activity from the retina).

Using this technique, we monitored the spontaneous activity in the retina-deprived tectum (Figure 6A) to compute the pairwise correlations between "naive" newborn neurons and the functionally mature neuronal population. Under enucleated conditions, the Ca^{2+}-event frequency of functionally mature neurons was not significantly different from that of functionally mature neurons in intact larvae (4 dpe; intact larvae: 0.0047 ± 0.001 Hz, n = 15, from 11 larvae; enucleated larvae: 0.0039 ± 0.001 Hz, n = 10, from six larvae; p = 0.70; Mann-Whitney

U test; Table S1). Likewise, the neuronal morphology of the newborn-labeled neurons, at 4 dpe, was not significantly affected by the enucleation process (total dendritic length in intact larvae: 363 ± 44 μm; total dendritic length in enucleated larvae: 447 ± 64 μm; p = 0.21; Mann-Whitney U test; n = 12 from intact larvae; n = 6 from enucleated larvae; Figures 6B and S4A). As previously observed [21], the correlations between functionally mature neurons were not significantly altered by the enucleations (40.8% ± 7.4% and 26.9% ± 6.4% of significant correlations for 4 dpe functionally mature neurons in intact and enucleated contexts; n = 3,969 and 1,913, respectively, from 11 and 6 larvae, respectively; distance: <20 μm; p = 0.19; Mann-Whitney U test; Figure 6C). Similarly, the compactness of the spatial structure of the correlations was weakly affected (0.49 ± 0.05 and 0.38 ± 0.04 for functionally mature neurons in intact and enucleated contexts, respectively; p = 0.15; Mann-Whitney U test; see STAR Methods). However, in the absence of retinal inputs, newborn neurons showed a significantly lower percentage of significant pairwise correlations with their functionally mature partners (54.2% ± 8.8% and 10.4% ± 4.3% of significant correlations for 4-dpe newborn neurons; distance: <20 μm; p = 1.0×10^{-4}; in intact and enucleated contexts; n = 15 and 10 from 11 and 6 larvae, respectively; Mann-Whitney U test; Figure 6D). Despite the decrease in the number of significant correlations, the few observed correlations showed average values not significantly different from those found in intact conditions (0.17 ± 0.02 and 0.11 ± 0.01 in intact and enucleated contexts, respectively; p = 0.18; Mann-Whitney U test). The spatial structure (topography) of these correlations was significantly sparser than those among functionally mature neurons (compactness: 0.62 ± 0.06 and 0.36 ± 0.03 for newborn neurons in intact and enucleated contexts, respectively; p = 0.013; Mann-Whitney U test; see STAR Methods). In support of these findings, we observed that the enucleations perturbed the correlations of neurons close to the proliferation site, whereas those of more distant neurons remained unaffected (Figure S4B). These results suggest that the integration of newborn neurons depends on the activity of pre-synaptic retinal inputs, promoting the emergence of pairwise correlations between newborn neurons and the functionally mature neuronal population.

DISCUSSION

The functional maturation of neuronal circuits has been previously studied [2, 4, 5, 9, 34]. However, how these circuits functionally assemble during development remains elusive. During development (between 5 and 8 dpf), the zebrafish optic tectum has already matured for its functional role (spatial detection and generation of adequate orienting behaviors). However, newborn neurons generated in the tectum's neurogenesis niche are continuously added to the functionally mature circuit [16, 18]. During the incorporation process, the combination of two-photon microscopy and optogenetics enables monitoring within the same optical plane the morphological and functional development of newborn neurons and a large population of functionally mature tectal neurons. By adapting an in vivo electroporation technique [22], we labeled neurons with immature morphology located next to neurogenic niches and lacking a defined neurotransmitter identity (neither GABAergic nor glutamatergic; Figure 1E). These newborn neurons progressively developed their dendritic arbors, reaching, at 4 dpe, a size corresponding to that of their mature state (Figure 1D) [23]. At this developmental stage, the newborn-labeled neurons had already gained neurotransmitter identity (GABAergic or glutamatergic). During their maturation, newborn neurons progressively drifted away from the neurogenic zone, probably passively pushed by new divisions of neuroepithelial progenitors (Figure 3A) [16, 18].

At 1 dpe, newborn neurons displayed intrinsic spontaneous Ca^{2+} transients with amplitudes and frequencies that did not significantly change during their maturation. Despite the functionally mature intrinsic dynamics at this early developmental stage, newborn neurons were not visually responsive, indicating that they receive no retinal inputs (Figure 2B). At 2 dpe, newborn neurons began to respond to visual stimuli in a low-amplitude, highly variable, and weakly tuned manner (Figures 2C–2F). At 3 dpe, they exhibited mature dendritic arbors, their visually induced responses became less variable, and their spatial receptive fields were tuned for specific regions of the field of view (Figures 2C–2G). At 4 dpe, they displayed mature receptive fields but still weak orientation and direction selectivity (Figures 2C–2J). This gradual maturation of the functional properties of newborn neurons during development contrasts that observed during adult neurogenesis in mice, where newborn neurons undergo a transient period of enhanced pre-synaptic and sensory responsiveness [2, 9, 10], a process required for their proper integration [35]. Furthermore, the incorporation process is much longer in adult mice than in zebrafish larvae (~8 weeks compared to 4 days). These differences could reflect the challenge of a newborn neuron to incorporate into an adult network relative to a more plastic developing circuit.

To monitor the functional integration of newborn neurons into biologically relevant neuronal assemblies [21, 31, 32], we examined the pairwise temporal correlations between the spontaneous activity of newborn and functionally mature neurons. From 1 to 2 dpe, newborn neurons were weakly correlated with their functionally mature counterparts (1–2 dpe; Figures 5C, 5D, S3A, and S3B). By 3–4 dpe, newborn neurons displayed correlated activity with functionally mature neurons at close physical distances, with characteristics similar to those of functionally mature neurons (Figures 5C and 5D). At this developmental stage, newborn-labeled neurons incorporate into topographically compact functional neuronal assemblies (Figures 5F, 5G, and S3C) [21].

Later (at 10 dpe), we observed a decrease in the number of the correlations between the newborn-labeled and the mature neurons (Figure 5E). Previously, we found that spontaneous assemblies group neurons with similar tuning curves rather than exclusively neighboring ones [21]. Therefore, the decrease in the number of correlations at 10 dpe might reflect the pruning of initially generated erroneous connections between nearby neurons with different visual receptive fields.

Activity-dependent mechanisms play an essential role in the development of the normal arborization, migration, and correct lamination of retinal inputs in rodents [36, 37] and participate in the development of the visual system in the *Xenopus* tadpole

[38]. However, their role in the incorporation of newborn neurons into established neuronal circuits remains unknown. We observed that enucleations performed just before the electroporations significantly reduced the percentage of significant correlations, suggesting that the integration of newborn neurons requires the activity of pre-synaptic retinal inputs (Figures 6D and 6E). Alternatively, it is possible that a subset of cells that trigger the activation of the neuronal assemblies require retinal input to develop normally. Yet, additional mechanisms (e.g., mechanical contact or molecular cues) may also play a role.

Overall, our study enabled the comprehensive description of the morphological, cell identity, and functional development of newborn neurons from an early immature state to functional incorporation into functionally mature circuits and the underlying mechanisms leading to the incorporation process. Interestingly, we observe that newborn neurons become visually responsive before showing strong correlations with neighboring neurons (Figures 2B and 5C). Within the context of the visual system of a developing vertebrate, our results suggest the following scenario: newborn neurons first generate unstable and weak connections with pre-synaptic inputs (retina). These initial connections enable synchronous activity patterns between newborn and functionally mature neurons, facilitating the increase in synaptic strength and stabilization of synapses between the two. This process then promotes the functional integration of newborn neurons into functionally mature sub-circuits and the acquisition of their functional identity (e.g., visual receptive field).

STAR★METHODS

Detailed methods are provided in the online version of this paper and include the following:

- KEY RESOURCES TABLE
- CONTACT FOR REAGENT AND RESOURCE SHARING
- EXPERIMENTAL MODEL AND SUBJECT DETAILS
- METHOD DETAILS
  - Electroporation of newborn neurons
  - Electroporation of mature neurons
  - Two-photon calcium imaging
  - Analysis of Ca^{2+} imaging data
  - Analysis of the pairwise correlations between neurons
  - Visual stimulation
  - Analysis of visually induced activity
  - Normalization of anatomical tectal coordinates
  - Detection of neuronal assemblies
  - Chronic longitudinal recordings
  - Single-eye enucleations
- QUANTIFICATION AND STATISTICAL ANALYSIS
  - Statistics
- DATA AND SOFTWARE AVAILABILITY
  - Software

SUPPLEMENTAL INFORMATION

Supplemental Information includes four figures and one table and can be found with this article online at http://dx.doi.org/10.1016/j.cub.2017.05.029.

AUTHOR CONTRIBUTIONS

J.B.-W. generated transgenic fish, developed the newborn-neuron-labeling technique, performed imaging experiments, wrote software, and analyzed data. V.C. participated in discussions, contributed in plasmids, performed confocal imaging experiments, and participated in neuronal tracings. S.A.R. and V.P.-S. participated in discussions, developed imaging analysis, wrote software, and built the experimental setup. A.J. participated in discussions, developed software for online drift compensation, and performed analyses of eye movements. J.B.-W. and G.S. conceived the experiments and wrote the manuscript.

ACKNOWLEDGMENTS

We thank A. Mizrahi and A. Marín-Burgin for comments on the manuscript; P. Gongal for editorial assistance; L. Bally-Cuif, S. Dieudonné, M. Kapsimali, S. Garel, B. Mathieu, and M. Privat for helpful discussions; and A. Torres-Herraez, M. Haudrechy, and M. Larroche for help during preliminary experiments. We are also grateful to the IBENS Imaging Facility. This work was supported by ERC grant StG 243106 to G.S., Boehringer-Ingelheim Fonds, Ministère de l'Enseignement Supérieur et de la Recherche, Fondation ARC dossier no. DOC20140601024, and a Labex MemoLife grant to J.B.-W. (ANR-10-LABX-54 MEMO LIFEANR-11-IDEX-0001-02 PSL* Research University).

Received: January 20, 2017
Revised: April 3, 2017
Accepted: May 9, 2017
Published: June 1, 2017

REFERENCES

1. Bond, A.M., Ming, G.L., and Song, H. (2015). Adult mammalian neural stem cells and neurogenesis: five decades later. Cell Stem Cell *17*, 385–395.
2. Livneh, Y., Adam, Y., and Mizrahi, A. (2014). Odor processing by adult-born neurons. Neuron *81*, 1097–1110.
3. Spitzer, N.C. (2006). Electrical activity in early neuronal development. Nature *444*, 707–712.
4. Carleton, A., Petreanu, L.T., Lansford, R., Alvarez-Buylla, A., and Lledo, P.-M. (2003). Becoming a new neuron in the adult olfactory bulb. Nat. Neurosci. *6*, 507–518.
5. Ge, S., Goh, E.L., Sailor, K.A., Kitabatake, Y., Ming, G.L., and Song, H. (2006). GABA regulates synaptic integration of newly generated neurons in the adult brain. Nature *439*, 589–593.
6. Toni, N., Teng, E.M., Bushong, E.A., Aimone, J.B., Zhao, C., Consiglio, A., van Praag, H., Martone, M.E., Ellisman, M.H., and Gage, F.H. (2007). Synapse formation on neurons born in the adult hippocampus. Nat. Neurosci. *10*, 727–734.
7. Faulkner, R.L., Jang, M.H., Liu, X.-B., Duan, X., Sailor, K.A., Kim, J.Y., Ge, S., Jones, E.G., Ming, G.L., Song, H., and Cheng, H.J. (2008). Development of hippocampal mossy fiber synaptic outputs by new neurons in the adult brain. Proc. Natl. Acad. Sci. USA *105*, 14157–14162.
8. Toni, N., Laplagne, D.A., Zhao, C., Lombardi, G., Ribak, C.E., Gage, F.H., and Schinder, A.F. (2008). Neurons born in the adult dentate gyrus form functional synapses with target cells. Nat. Neurosci. *11*, 901–907.
9. Marín-Burgin, A., Mongiat, L.A., Pardi, M.B., and Schinder, A.F. (2012). Unique processing during a period of high excitation/inhibition balance in adult-born neurons. Science *335*, 1238–1242.
10. Danielson, N.B., Kaifosh, P., Zaremba, J.D., Lovett-Barron, M., Tsai, J., Denny, C.A., Balough, E.M., Goldberg, A.R., Drew, L.J., Hen, R., et al. (2016). Distinct contribution of adult-born hippocampal granule cells to context encoding. Neuron *90*, 101–112.
11. Gahtan, E., Tanger, P., and Baier, H. (2005). Visual prey capture in larval zebrafish is controlled by identified reticulospinal neurons downstream of the tectum. J. Neurosci. *25*, 9294–9303.

12. Barker, A.J., and Baier, H. (2015). Sensorimotor decision making in the zebrafish tectum. Curr. Biol. *25*, 2804–2814.
13. Nikolaou, N., and Meyer, M.P. (2015). Lamination speeds the functional development of visual circuits. Neuron *88*, 999–1013.
14. Niell, C.M., and Smith, S.J. (2005). Functional imaging reveals rapid development of visual response properties in the zebrafish tectum. Neuron *45*, 941–951.
15. Friedrich, R.W., Jacobson, G.A., and Zhu, P. (2010). Circuit neuroscience in zebrafish. Curr. Biol. *20*, R371–R381.
16. Galant, S., Furlan, G., Coolen, M., Dirian, L., Foucher, I., and Bally-Cuif, L. (2016). Embryonic origin and lineage hierarchies of the neural progenitor subtypes building the zebrafish adult midbrain. Dev. Biol. *420*, 120–135.
17. Ito, Y., Tanaka, H., Okamoto, H., and Ohshima, T. (2010). Characterization of neural stem cells and their progeny in the adult zebrafish optic tectum. Dev. Biol. *342*, 26–38.
18. Recher, G., Jouralet, J., Brombin, A., Heuzé, A., Mugniery, E., Hermel, J.-M., Desnoulez, S., Savy, T., Herbomel, P., Bourrat, F., et al. (2013). Zebrafish midbrain slow-amplifying progenitors exhibit high levels of transcripts for nucleotide and ribosome biogenesis. Development *140*, 4860–4869.
19. Orger, M.B., Kampff, A.R., Severi, K.E., Bollmann, J.H., and Engert, F. (2008). Control of visually guided behavior by distinct populations of spinal projection neurons. Nat. Neurosci. *11*, 327–333.
20. Preuss, S.J., Trivedi, C.A., vom Berg-Maurer, C.M., Ryu, S., and Bollmann, J.H. (2014). Classification of object size in retinotectal microcircuits. Curr. Biol. *24*, 2376–2385.
21. Romano, S.A., Pietri, T., Pérez-Schuster, V., Jouary, A., Haudrechy, M., and Sumbre, G. (2015). Spontaneous neuronal network dynamics reveal circuit's functional adaptations for behavior. Neuron *85*, 1070–1085.
22. Kera, S.A., Agerwala, S.M., and Horne, J.H. (2010). The temporal resolution of in vivo electroporation in zebrafish: a method for time-resolved loss of function. Zebrafish *7*, 97–108.
23. Niell, C.M., Meyer, M.P., and Smith, S.J. (2004). In vivo imaging of synapse formation on a growing dendritic arbor. Nat. Neurosci. *7*, 254–260.
24. Robles, E., Smith, S.J., and Baier, H. (2011). Characterization of genetically targeted neuron types in the zebrafish optic tectum. Front. Neural Circuits *5*, 1.
25. Nevin, L.M., Robles, E., Baier, H., and Scott, E.K. (2010). Focusing on optic tectum circuitry through the lens of genetics. BMC Biol. *8*, 126.
26. Gabriel, J.P., Trivedi, C.A., Maurer, C.M., Ryu, S., and Bollmann, J.H. (2012). Layer-specific targeting of direction-selective neurons in the zebrafish optic tectum. Neuron *76*, 1147–1160.
27. Nikolaou, N., Lowe, A.S.S., Walker, A.S.S., Abbas, F., Hunter, P.R.R., Thompson, I.D.D., and Meyer, M.P.P. (2012). Parametric functional maps of visual inputs to the tectum. Neuron *76*, 317–324.
28. Pérez-Schuster, V., Kulkarni, A., Nouvian, M., Romano, S.A., Lygdas, K., Jouary, A., Dippopa, M., Pietri, T., Haudrechy, M., Candat, V., et al. (2016). Sustained rhythmic brain activity underlies visual motion perception in zebrafish. Cell Rep. *17*, 1098–1112.
29. Easter, S.S., Jr., and Stuermer, C.A. (1984). An evaluation of the hypothesis of shifting terminals in goldfish optic tectum. J. Neurosci. *4*, 1052–1063.
30. Gaze, R.M., Keating, M.J., and Chung, S.H. (1974). The evolution of the retinotectal map during development in Xenopus. Proc. R. Soc. Lond. B Biol. Sci. *185*, 301–330.
31. Kenet, T., Bibitchkov, D., Tsodyks, M., Grinvald, A., and Arieli, A. (2003). Spontaneously emerging cortical representations of visual attributes. Nature *425*, 954–956.
32. Miller, J.-E.K., Ayzenshtat, I., Carrillo-Reid, L., and Yuste, R. (2014). Visual stimuli recruit intrinsically generated cortical ensembles. Proc. Natl. Acad. Sci. USA *111*, E4053–E4061.
33. Sporns, O., Tononi, G., and Edelman, G.M. (2000). Connectivity and complexity: the relationship between neuroanatomy and brain dynamics. Neural Netw. *13*, 909–922.
34. Ko, H., Cossell, L., Baragli, C., Antolik, J., Clopath, C., Hofer, S.B., and Mrsic-Flogel, T.D. (2013). The emergence of functional microcircuits in visual cortex. Nature *496*, 96–100.
35. Lin, C.W., Sim, S., Ainsworth, A., Okada, M., Kelsch, W., and Lois, C. (2010). Genetically increased cell-intrinsic excitability enhances neuronal integration into adult brain circuits. Neuron *65*, 32–39.
36. Mrsic-Flogel, T.D., Hofer, S.B., Creutzfeldt, C., Cloëz-Tayarani, I., Changeux, J.-P., Bonhoeffer, T., and Hübener, M. (2005). Altered map of visual space in the superior colliculus of mice lacking early retinal waves. J. Neurosci. *25*, 6921–6928.
37. Penn, A.A., Riquelme, P.A., Feller, M.B., and Shatz, C.J. (1998). Competition in retinogeniculate patterning driven by spontaneous activity. Science *279*, 2108–2112.
38. Pratt, K.G., Hiramoto, M., and Cline, H.T. (2016). An evolutionarily conserved mechanism for activity-dependent visual circuit development. Front. Neural Circuits *10*, 79.
39. Satou, C., Kimura, Y., Hirata, H., Suster, M.L., Kawakami, K., and Higashijima, S. (2013). Transgenic tools to characterize neuronal properties of discrete populations of zebrafish neurons. Development *140*, 3927–3931.
40. Sugiyama, M., Sakaue-Sawano, A., Iimura, T., Fukami, K., Kitaguchi, T., Kawakami, K., Okamoto, H., Higashijima, S., and Miyawaki, A. (2009). Illuminating cell-cycle progression in the developing zebrafish embryo. Proc. Natl. Acad. Sci. USA *106*, 20812–20817.
41. D'Souza, J., Hendricks, M., Le Guyader, S., Subburaju, S., Grunewald, B., Scholich, K., and Jesuthasan, S. (2005). Formation of the retinotectal projection requires Esrom, an ortholog of PAM (protein associated with Myc). Development *132*, 247–256.
42. Pologruto, T.A., Sabatini, B.L., and Svoboda, K. (2003). ScanImage: flexible software for operating laser scanning microscopes. Biomed. Eng. Online *2*, 13.
43. Brainard, D.H. (1997). The psychophysics toolbox. Spat. Vis. *10*, 433–436.
44. Romano, S.A., Pérez-schuster, V., Jouary, A., Candeo, A., Boulanger-Weill, J., and Sumbre, G. (2017). A computational toolbox and step-by-step tutorial for the analysis of neuronal population dynamics in calcium imaging data. bioRxiv. http://dx.doi.org/10.1101/103879.
45. Turner, M.H., Ullmann, J.F.P., and Kay, A.R. (2012). A method for detecting molecular transport within the cerebral ventricles of live zebrafish (Danio rerio) larvae. J. Physiol. *590*, 2233–2240.
46. Kwan, K.M., Fujimoto, E., Grabher, C., Mangum, B.D., Hardy, M.E., Campbell, D.S., Parant, J.M., Yost, H.J., Kanki, J.P., and Chien, C.B. (2007). The Tol2kit: a multisite gateway-based construction kit for Tol2 transposon transgenesis constructs. Dev. Dyn. *236*, 3088–3099.
47. Balciunas, D., Wangensteen, K.J., Wilber, A., Bell, J., Geurts, A., Sivasubbu, S., Wang, X., Hackett, P.B., Largaespada, D.A., McIvor, R.S., and Ekker, S.C. (2006). Harnessing a high cargo-capacity transposon for genetic applications in vertebrates. PLoS Genet. *2*, e169.
48. Sato, Y., Kasai, T., Nakagawa, S., Tanabe, K., Watanabe, T., Kawakami, K., and Takahashi, Y. (2007). Stable integration and conditional expression of electroporated transgenes in chicken embryos. Dev. Biol. *305*, 616–624.
49. Subach, O.M., Cranfill, P.J., Davidson, M.W., and Verkhusha, V.V. (2011). An enhanced monomeric blue fluorescent protein with the high chemical stability of the chromophore. PLoS ONE *6*, e28674.
50. Tawk, M., Bianco, I.H., and Clarke, J.D. (2009). Focal electroporation in zebrafish embryos and larvae. Methods Mol. Biol. *546*, 145–151.
51. Scott, E.K., and Baier, H. (2009). The cellular architecture of the larval zebrafish tectum, as revealed by gal4 enhancer trap lines. Front. Neural Circuits *3*, 13.
52. Pietri, T., Romano, S.A., Pérez-Schuster, V., Boulanger-Weill, J., Candat, V., and Sumbre, G. (2017). The emergence of the spatial structure of tectal spontaneous activity is independent of visual inputs. Cell Rep. *19*, 939–948.

53. Tseng, Q., Duchemin-Pelletier, E., Deshiere, A., Balland, M., Guillou, H., Filhol, O., and Théry, M. (2012). Spatial organization of the extracellular matrix regulates cell-cell junction positioning. Proc. Natl. Acad. Sci. USA *109*, 1506–1511.

54. Del Bene, F., Wyart, C., Robles, E., Tran, A., Looger, L., Scott, E.K., Isacoff, E.Y., and Baier, H. (2010). Filtering of visual information in the tectum by an identified neural circuit. Science *330*, 669–673.

55. Zhang, B.-B., Yao, Y.Y., Zhang, H.F., Kawakami, K., and Du, J.L. (2017). Left habenula mediates light-preference behavior in zebrafish via an asymmetrical visual pathway. Neuron *93*, 914–928.e4.

56. Fernandes, A.M., Fero, K., Arrenberg, A.B., Bergeron, S.A., Driever, W., and Burgess, H.A. (2012). Deep brain photoreceptors control light-seeking behavior in zebrafish larvae. Curr. Biol. *22*, 2042–2047.

STAR★METHODS

KEY RESOURCES TABLE

REAGENT or RESOURCE	SOURCE	IDENTIFIER
Chemicals, Peptides, and Recombinant Proteins		
Pancuronium	Tocris Bioscience	Cat. No. 0693
Dextran, Fluorescein, 3000 MW, Anionic, Lysine Fixable	Molecular Probes	D-3306
Experimental Models: Organisms/Strains		
Zebrafish:Tg(gad1b:GFP;vglut2a:loxP-DsRed-loxP-GFP)	[39]	RRID: ZDB-ALT-131127-6 and ZDB-ALT-110413-5
Zebrafish: Tg(huC:GCaMP5G)^{ens102Tg}	[28]	RRID: ZDB-ALT-161209-7
Zebrafish: Tg(EF1:mAG-hGem(1/100);huC:GCaMP5G)	[28, 40]	RRID: ZDB-FISH-150901-10376 and ZDB-ALT-161209-7
Recombinant DNA		
Tol2-*huC*:Gal4	[41]	N/A
Tol2-*2xUAS*:dTomato-CAAX	This paper	N/A
Tol2-*10xUAS*:tagBFP2CAAX	This paper	N/A
Software and Algorithms		
MATLAB 2013b (Data analysis)	MathWorks	http://www.mathworks.com
ScanImage 3.8 (Calcium recordings acquisition)	[42]	http://scanimage.vidriotechnologies.com
Psychtoolbox-3 (Visual stimulation)	[43]	http://psychtoolbox.org/
Promax algorithm (detection of neuronal assemblies)	[21, 44]	http://www.zebrain.biologie.ens.fr/codes/
ImageJ (Imaging analysis)	NIH	https://imagej.nih.gov/ij/
Imaris (Neuronal reconstruction)	Bitplane	http://www.bitplane.com/

CONTACT FOR REAGENT AND RESOURCE SHARING

Further information and requests for resources and reagents should be directed to and will be fulfilled by the Lead Contact German Sumbre (sumbre@biologie.ens.fr)

EXPERIMENTAL MODEL AND SUBJECT DETAILS

Larvae were raised up to 10 dpf, in 0.5x E3 embryo medium and kept under a 14/10 hr on/off light cycle. After 5 dpf, larvae were fed with paramecia. All experiments were approved by the Comité d'Éthique pour l'Expérimentation Animale Charles Darwin (03839.03).

Calcium imaging experiments were performed on *Tg(huC:GCaMP5)* zebrafish larvae [28], in Nacre background (mitfa$^{-/-}$). For assessing the neurotransmitter type of newborn neurons we used *Tg(vglut2a:loxP-DsRed-loxP-GFP)* crossed with *Tg(gad1b:GFP)* zebrafish lines [39]. To visualize dividing cells we used *Tg(EF1:mAG-hGem(1/100))* line [40] *crossed with Tg(huC:GCaMP5).*

METHOD DETAILS

Electroporation of newborn neurons

Four dpf larvae were embedded in 2% low-melting agarose (Invitrogen, USA) in Evans solution (134 mM NaCl, 2.9 mM KCl, 2.1 mM $CaCl_2$, 1.2 mM $MgCl_2$, 10 mM glucose and 10 mM HEPES at 290 mOsm and pH 7.8) and covered with E3 medium. The electroporation device consisted of two 125 μm platinum-iridium (90/10%) electrodes (GoodFellow, UK) spaced by ~1 mm and mounted on a micro-manipulator. Glass capillaries (1.0 mm outer diameter, 0.5 mm inner diameter, without filament, FHC, USA) were pulled using a Kopf 720 puller (David Kopf Instruments, USA) and back loaded with DNA solution. The tip was broken off with forceps to a diameter of ~10 μm. For visualization of the injected solution, phenol red was added to the solution (0.05%). The solution was injected by several pressure pulses until the red solution could be clearly identifiable in the tectal ventricle [45], using a pneumatic picopump (Pv 820, World Precision Instrument). Immediately after the injection, one electric square pulse (4 ms, 17 V) was delivered using a SD9 Stimulator (Grass Technologies, USA) and monitored using an oscilloscope (Tektronic, RDS 2022C, USA).

For morphological and functional analysis, we used Tol2-*huC:*Gal4 (gift from S. Jesuthasan, Temasek Life Sciences Laboratory, Singapore) [41]. Tol2-*2xUAS*:dTomatoCAAX and *2xUAS*:Transposase vectors. The cDNA containing two *UAS* repeats upstream of dTomato fused to the RAS CAAX sequence for membrane targeting was chemically synthesized (Eurofins Genomics, Germany), and ligated into a Tol2 destination vector [46]. The *2xUAS*:Transposase vector was generated using pT3TS-Tol2 containing the medaka transposase as a destination vector [47]. The *2xUAS* sequence was PCR amplified from Tol2-*2xUAS*:dTomatoCAAX and ligated upstream of the Transposase open reading frame. The co-electroporation of a Transposase has been shown to enhance

the stable genomic integration of transgenes flanked by Tol2 sequences [48]. The injection solution consisted of Tol2-*2xUAS*:dTomatoCAAX (2 μg/μL), Tol2-*huC:*Gal4 and *2xUAS*:Transposase (1 μg/μL), in ddH_20.

For the determination of the neurotransmitter identity, we generated a Tol2-*10xUAS:*mTagBFP2CAAX vector by successive ligations. mTagBFP2 [49] was PCR amplified using primers containing a 3′ CAAX sequence and ligated into a Tol2-*10xUAS* destination vector [46]. The injection solution consisted of Tol2-*10xUAS*:mTagBFP2CAAX vector (2 μg/μL), Tol2-*huC:*Gal4 and *2xUAS*:Transposase (1 μg/μL), and phenol red (0.05%) in ddH_20.

Electroporation of mature neurons

Electroporations were performed at 5 dpf as previously described [50] using a fluorescent dextran (D-3306, Molecular Probes). We used borosilicate glass capillaries (Harvard Apparatus, GC150F-15) forged using a custom-made vertical puller to obtain a tip diameter of ~1 μm. Capillaries were inserted into the mature tectal region of the periventricular layer of the optic tectum using a micromanipulator.

Two-photon calcium imaging

The imaging set-up was based on a MOM system (Sutter, USA) with a 25x NA 1.05 Olympus objective and a Mai-Tai DeepSee Ti:sapphire laser tuned at 920 nm. The output power at the focal plane was less than 3 mW. The green GCaMP5G and the red dTomato emitted photons were collected in epi and deflected toward dedicated PMTs (photo-multiplier) via a 670dcrx dichroic mirror (Chroma, USA). Infra-red light was filtered from the emission path by a FF01-680 short-path filter. The wavelength of the emitted fluorescence was separated into two channels (green and red) by a FF562-Di03 dichroic mirror. Band-pass filters FF01-520/70 (green) and FF01-607/70 (red) were placed before the PMTs (H1070, GaAsP from Hamamatsu, Japan). These filters assured accurate spectral separation to resolve both calcium dynamics and the morphological features of the newborn-labeled neurons. All filters were Semrock, USA, unless otherwise noted. The emission signal was pre-amplified with a SR-570 (Stanford Research Systems, USA) and acquired using ScanImage 3.8 [42].

Due to agarose dilatation during the experiments, drifts in the Z plane may occur. To that end, we performed a Z axis compensation in realtime: every 100 frames an average image was generated and cross-correlated with 3 reference images acquired before the onset of the experiment (the recording optical plane and 2 other planes separated by 2.44 μm below and above the recording plane). If the correlation was higher with the dorsal or ventral optical planes an automatic compensation was performed by displacing the objective by increments of 0.44 μm until the correlation of the running average was again maximal with the reference optical plane.

To reconstruct the neuronal morphology of newborn-labeled neurons, we recorded a Z stack of several optical planes, comprising the entire morphology of the neuron, and separated every 1 μm. The images of each optical plane within the stack corresponded to an average of 10 acquired images. For the quantification of the total dendritic length, we used a semi-automatic neuronal tracing algorithm based on Imaris, after a MATLAB pre-processing step to remove the skin and facilitate the detection process. Only larvae with a single labeled neuron were kept for further analyses. For the determination of the neuronal type according to its morphology, we rotated the 3D stacks by ~45° as previously described [51]. The rotation enables visualizing the neurons' morphology from a view orthogonal to the arborization planes, important for the proper morphological classification.

Analysis of Ca^{2+} imaging data

Processing of the GCaMP5 fluorescence signal was performed as previously described [21, 28, 44, 52]. Important steps are summarized below.

The series of images during a given experiment were saved as TIFF stacks. Stacks were registered using the ImageJ plugin Template Matching [53], in combination with a custom-made algorithm in MATLAB to further smooth the registration. When the real-time Z axis drifting compensation failed, videos were systematically discarded.

Movement artifacts were detected according to large deviations in the cross-correlation between successive frames. All frames with large deviations (z-score smaller than −2) were then manually inspected. Due to the agarose elasticity, the imaging plane almost invariantly returned to its original position, after observing movement artifacts. If this was not the case, the complete experiment was discarded. Artifact episodes rarely exceeded 5 consecutive frames in non-paralyzed larvae. For the subsequent data analysis, we did not include frames showing moving artifacts.

Regions of interest (ROIs) corresponding to the imaged neurons were semi-automatically detected on a morphological basis by the analysis of time-averaged registered stacks. Digital imaging processing techniques were implemented in a custom-made program, producing putative ROIs layouts that were manually curated thereafter. The algorithm first identified neuronal ROIs that corresponded to individual nuclei. The latter were detected by local fluorescence intensity wells. Local minima were detected by applying a user-defined threshold to the extended-minima transform of the resulting image. Eventually, neuronal boundaries were obtained by watershed segmentation.

Statistical significance of single-neuron calcium transients was calculated in an adaptive and unsupervised manner. In this framework, any event in the fluorescence time series data belongs to either a neuronal activity process, A, or an underlying noisy baseline, B. We devised a data-driven model to discriminate with a desired degree of confidence between these two sources. Biophysical constraints of the fluorescent calcium indicator were taken into account (GCaMP5G fluorescence decay time constant: 1.44 s). Then, we applied a Bayesian odds ratio estimation framework. Non-significant portions of the ΔF/F traces were then set equal to 0 in all subsequent analysis.

Analysis of the pairwise correlations between neurons

To calculate the spontaneous Pearson's pairwise correlations between neurons, we performed recordings of tectal activity in the absence of external sensory stimulation, for one-hour periods [21]. We found that the level of correlations (for all conditions) increased as the length of the experiments was incremented. However, the level of correlations reached a plateau at ~40 min. These plateaux did not represent a decrease in the number of events with respect to the beginning of the experiments (the percentage of calcium events during the first 30 min was not significantly different from the percentage of events in the last 30 min, 48.44% of events were observed in the first half and 51.56% in the second half, p = 0.06, n = 27 in intact conditions).

From these patterns of spontaneous activity, we computed the temporal Pearson's linear correlation *p* for all neuronal pairs. For a pair of neuron *i* and *j*, *p(i,j)* was computed using significant ΔF/F values (see Analysis of Ca^{2+} imaging data). *p(i,j)* is the covariance of *Xi* and *Xj* divided by the product of their standard deviations. Significant correlations were extracted by thresholding correlation values. The threshold was calculated based on a surrogate dataset where the spontaneous Ca^{2+}-events times stamps were randomly permuted. We then calculated the 99.9^{th} percentile value of the distribution of the correlations which was defined as the threshold for each dataset (Figure 2B). The mean value of the threshold was 0.059 ± 0.003 (mean ± SEM) for n = 44 recordings. All correlations greater than this threshold were considered as significant.

We found that these thresholds were not significantly different between recordings performed at different dpe (1-4 dpe, p = 0.07, ANOVA), except for the enucleated experiments at 4 dpe (p = 0.002, Mann-Whitney U test). Despite their similarity, we tested whether these different thresholds could have an impact in our results. For this, we recalculated the data showed in Figure 5C of the manuscript, according to two different thresholds (the highest: 0.0625 and lowest: 0.035 found in the data). We found that these two extreme thresholds used for the calculation of the significant correlations did not alter our previous findings. Therefore, levels of variations in the spontaneous activity found at the different conditions, do not influence the essence of our conclusions.

The average number of significant Ca^{2+} events varied between neuronal types (newborn-labeled and functionally mature) and the different conditions (1-4 dpe, in normal and enucleated larvae, see Table S1). Note that the number of significant Ca^{2+} events do not follow the tendencies observed in the percentage of significant correlations observed in Figure 5C. Overall, our results suggest that the level of significant correlations depends mainly on the level of synchronization between neurons rather than their level activity.

To plot the relationship between the correlations and the physical distance between the correlated neurons, we calculated the pairwise neuron-to-neuron physical distances (from the centroids of each neuron). The distributions were established by binning correlation values or the percentage of significant correlations among all pairwise correlations, by 20 μm bins (from 0 to 200 μm). To compare the difference between newborn and mature neurons, we used the Mann-Whitney U test for each of the distance bins. Average distributions for mature or newborn-labeled neurons were obtained for each larva by averaging all mature or newborn-labeled neurons' distributions, respectively. Average distributions for each day (from 1 to 4 dpe) were obtained by averaging distributions for mature or newborn-labeled neurons arising from larva of the same age. For visualization purposes, distributions were smoothed by a shape-preserving piecewise cubic interpolation.

Mature neurons were detected by the level of pairwise correlation values across distance using the X^2 distance:

$$X^2 = \sum_{i=1}^{n} \left(\frac{(x_i - y_i)^2}{x_i + y_i} \right).$$

We calculated the X^2 distance between the distribution of the percentage of significant correlations along distance of each neuron (*x*) with the average distribution of all neurons in a given recorded larva (*y*). Neurons, with a X^2 distance smaller than the average X^2 distance for each larva plus one standard deviation were considered as mature. Neurons with a large X^2 distance were clustered next to the neurogenesis region (Figure S3E), suggesting that they are indeed immature neurons not yet incorporated into the functional tectal circuit.

Visual stimulation

Larvae were embedded in 2% low-melting agarose (Invitrogen, USA) in E3 embryo medium and placed on an elevated stage within a custom-made cylindrical chamber filled with E3 embryo medium without the use of paralyzer agents or anesthetics. The elevated stage enables the larva to have an unobstructed view of the entire field of view of the projected stimuli. Visual stimuli were projected on a screen (#216 White Diffusion, Rosco Cinegel, UK) placed around the wall of the recording chamber, using a pico-projector (refresh rate: 60 Hz, P4X, AAXA, USA), covering a field of view of ~90° x 40° (horizontal x vertical). The opposite side of the recording chamber was covered with low-reflection black paper (T137-2,0, ThorLabs, USA) to prevent the stimulus reflection. To avoid the interference the GCaMP5G emission signal (peaking at 547 nm and filtered using a 520/70 band-pass filter), by the visual stimuli, we only used the projector's red LED (~620 nm). In addition, a long-pass filter (BLP01-561, Semrock, USA) was placed in the front of the projector. Larvae were carefully aligned to the projector with the help of a custom-made program that mapped azimuth angles on the chamber's projection screen. In order to minimize projection distortions due to the cylindrical chamber, we calibrated the projection to compensate as much as possible for the chamber's curvature.

To study the responsiveness of newborn and mature neurons, we presented to the larvae 5° light spots at 36 different positions of the field of view (90° horizontal x 40° vertical coverage, 9 × 4 light spots separated by 5°), lasting 1 s and centered at 140° relative to the larva's midline. The light spots were repeated 20 times at each of the different positions. Then, 4° wide x 90° long moving bars were presented in the four cardinal directions moving at 45 °/s covering 90° x 90° of the field of view (4 repetitions per direction). In all

cases, the order of the stimuli positions and directions were randomized, and the inter-stimulus interval set at 6 s (from onset to onset). Overall, a total of 16 moving bars (4 per cardinal direction) and 720 light spots (20 per position) were presented per experiment.

To compute the spatial tuning curves of newborn and mature tectal neurons, we presented to the larvae 5° light spots at 15 different positions of the field of view (90° horizontal coverage, same azimuthal plane), lasting 1 s and centered at 140° relative to the larva's midline. The light spots were presented 8 times at each of the different positions. The azimuth of the stimuli was chosen according to the maximal neuronal response in the imaged optical plane. In all cases, the order of the stimulus positions and directions were randomized. The inter-stimulus interval was 7 s (from onset to onset). Overall, a total of 120 light spots (8 per position) were presented per experiment.

The 2% low-melting agarose used to restrain the larva under the microscope was sufficient to prevent eye movements. The amplitude of eye rotations under these conditions was not significantly different from that of paralyzed larvae (0.3 mg/mL pancuronium bromide diluted in agarose [28], agarose restrained: 0.62° ± 0.37°, paralyzed: 1.2° ± 0.5°, $p = 0.71$, Mann-Whitney U test), and were significantly lower than that in conditions in which the agarose was removed around the eyes (agarose restrained: 0.62° ± 0.37°, eyes free to move: 9° ± 1.8°, $p < 0.001$, Mann-Whitney U test).

To compute the direction and the orientation selectivity we presented to the larvae sinusoidal gratings (0.01 cycles/°, 2 cycles/s) moving in eight different directions. The order of the different stimuli directions was randomly interleaved, and each direction was presented 8 times. The stimulus lasted for 5 s and the inter-stimulus interval was of 15 s. A Gaussian mask was overlaid on the stimulus to minimize border effects. The stimuli were centered at 140° relative to the larva's midline and the azimuthal plane was chosen according to the maximal neuronal response in the imaged optical plane. The inter-stimulus interval was 20 s (from onset to onset). Overall, we presented to the larvae a total of 64 drifting gratings per experiment. All visual stimuli were programmed using Psychtoolbox [43] for MATLAB and synchronized with ScanImage 3.8 using a TTL pulse delivered by a MATLAB-controlled I/O board (ActiveWire, Inc, USA) or an Arduino Uno (Arduino, Italy).

Analysis of visually induced activity

Evaluation of the neuronal responsiveness, the spatial tuning curves and direction and orientation selectivity were computed using the thresholded ΔF/F data: 0 for values non-significantly different from noise, > 0 values corresponding to the amplitude of significant Ca^{2+} transients (ΔF/F).

Significantly responsive neurons were selected by averaging the baseline activity from 1 s to 0.5 s time window prior to the presentation of each stimulus. Visually induced activity was averaged during 3 s following the stimulus presentation. Distribution medians pre- and post-stimuli were compared using a non-parametric Mann-Whitney U test. Neurons with p values smaller than 0.01 (those that exhibited a consistent and significant increase in fluorescence during periods of stimulus presentation compared to the preceding baseline) were considered as visually responsive.

When spontaneous activity was not recorded, we defined mature neurons based on the normalized coordinates and the X^2 distance metric previously established (Figure S3E). We computed the average distance in normalized coordinates corresponding to a X^2 distance equal to the average plus 1 standard deviation, from that observed in the experiments in which we recorded spontaneous tectal activity (0.089 ± 0.003, n = 44 recordings). We considered neurons as mature if they were significantly responsive with a probability bigger than 0.05 (when using either light spots or drifting gratings) and with normalized positions > 0.089.

To calculate the spatial tuning curves, the responses to the light spots were evaluated by measuring the peak amplitude (ΔF/F) of the Ca^{2+} transients during a time window corresponding to the duration of the stimulus plus 2 s following the off set of the stimulus. The amplitude of the Ca^{2+} transients induced by a light spot at the same angular position was averaged across trials. The receptive field size was calculated as the number of angular positions eliciting Ca^{2+} responses in at least 50% of the trials, multiplied by the size of the light-spot stimulus. The coefficient of variation was estimated for the peak responses across the different trials to assess the trial-to-trial variability.

The sharpness of the spatial tuning curves was evaluated by fitting light-spot responses to a Gaussian function. The sharpness was calculated as the ratio of the half-maximum amplitude divided by the half-width at half-maximum of the fitted curve. Because of the poor fitting efficiency at 1-2 dpe (the tuning curves were not yet developed at this early developmental stage), sharpness was computed only for 3-4 dpe newborn-labeled neurons.

Visual responses to moving gratings were evaluated by measuring the peak amplitude of the Ca^{2+} transients during the period corresponding to the stimulus presentation minus 1 s, to exclude the off responses. The amplitudes of the Ca^{2+} transients induced by moving gratings presented at each angular position were averaged across trials and shown as polar plots (Figure 2I). The coefficient of variation was estimated for the peak responses across the different trials to assess the trial-to-trial variability. To compute orientation and direction selectivity, each measured tuning curve was fitted with the sum of two circular Gaussian functions where the peaks were constrained to be 180° apart (Von Mises distributions). The maximal angular response θ_{pref} was the angle corresponding to maximum of the fitted distributions. Orientation and direction selectivity were computed as previously described [27]:

$$OSI = \frac{(Pref_{Ori} - Orth)}{(Pref_{Ori} + Orth)},$$

where

$$Pref_{Ori} = Resp(\theta_{Pref}) \text{ and } Orth = Resp\left(\theta_{Pref} + \frac{\pi}{2}\right),$$

$$DSI = \frac{(Pref_{dir} - Opp)}{(Pref_{dir} + Opp)},$$

where

$$Pref_{dir} = Resp(\theta_{Pref}) \text{ and } Opp = Resp(\theta_{Pref} + \pi).$$

Orientation and direction selectivity indexes, and coefficient of variation average values were obtained for each larva by averaging distributions of all mature or newborn-labeled neurons.

Normalization of anatomical tectal coordinates

To compare functional features between larvae and different developmental stages, we used a method to determine the physical positions of tectal neurons in anatomically normalized tectal coordinates [21]. The Cartesian centroid coordinates of each neuron were projected along a manually drawn caudo-rostral axis along the PVZ tectal layer. The length of this axis was then normalized. To image similar optical planes across larvae, we used anatomical landmarks such as the parallel fibers of the cerebellum.

Detection of neuronal assemblies

Groups of neurons with significantly correlated spontaneous activity patterns were detected using the *PCA-promax* algorithm [21]. The probability of integration of neurons into such groups was computed as the number of mature and labeled newborn neurons contained into neuronal assemblies divided by the total number of mature and newborn neurons, respectively. The maximal PC loadings were calculated for each neuron, both for mature and newborn-labeled neurons. Average values were obtained for each larva by averaging mean correlations of all mature or newborn-labeled neurons belonging to a given assembly. Average values obtained for each larva were averaged for each developmental stage (1-4 dpe).

The compactness of the neuronal assemblies was calculated according to [21]. Briefly, the compactness is the density or sparseness of the assembly: a dimensionless, data-independent, normalized index that enabled us to unbiasedly compare across experiments (intact and enucleated). We estimated the assembly's topography density map using morphological masks. The region occupied by the assembly was defined as the region encompassed by the contour line that corresponds to a density value of half the maximal density. We defined the compactness index as the proportion of assembly neurons that reside within the borders of this contour.

Chronic longitudinal recordings

To compare the spatial receptive fields across different developmental stages, we monitored the eye positions after agarose immobilization and compared this to the previous day position. Larvae with a difference in eyes angular position of 20° between successive recordings were discarded for the analysis of the displacement of their tuning curves (Figure 3B). To minimize eye position variability across larvae and developmental stages, we anesthetized the larvae on ice before placing them in agarose.

Single-eye enucleations

For this purpose 3.5 dpf larvae were embedded in 2% low-melting agarose and immersed in E3 medium. The petri dish containing the larvae was then placed on ice, until mechanical stimulation of the tail did not elicit movement. Enucleations were performed immediately using a curved insect pin. Following the procedure, larvae were freed from agarose and placed into ~4°C Ringer solution to avoid heat shock. After one hour, the solution reached room temperature and larvae were placed in the incubator overnight until electroporation was performed the next morning. Larvae were then returned to E3 medium. Survival was comparable to that of non-enucleated controls (> 95%) confirming previous reports in which development of the larva was no affected by single-eye enucleations [52, 54–56].

QUANTIFICATION AND STATISTICAL ANALYSIS

Statistics

For two-group comparisons we used the Mann-Whitney U test, unless otherwise stated. For comparison among multiple newborn-labeled neuron groups, we used the Kruskal-Wallis test, unless otherwise stated. For chronic comparison of neuronal properties, we used the one-tailed Wilcoxon rank sum test. p values lower than 0.05 were considered to be statistically significant. All results are represented as mean ± SEM. The "n" represents the number of neurons (newborn-labeled or mature).

DATA AND SOFTWARE AVAILABILITY

Software

All the developed software for data analysis and visual stimulation was coded in MATLAB. The codes will be made available upon request.

Current Biology, Volume *27*

Supplemental Information

Functional Interactions between Newborn and Mature Neurons Leading to Integration into Established Neuronal Circuits

Jonathan Boulanger-Weill, Virginie Candat, Adrien Jouary, Sebastián A. Romano, Verónica Pérez-Schuster, and Germán Sumbre

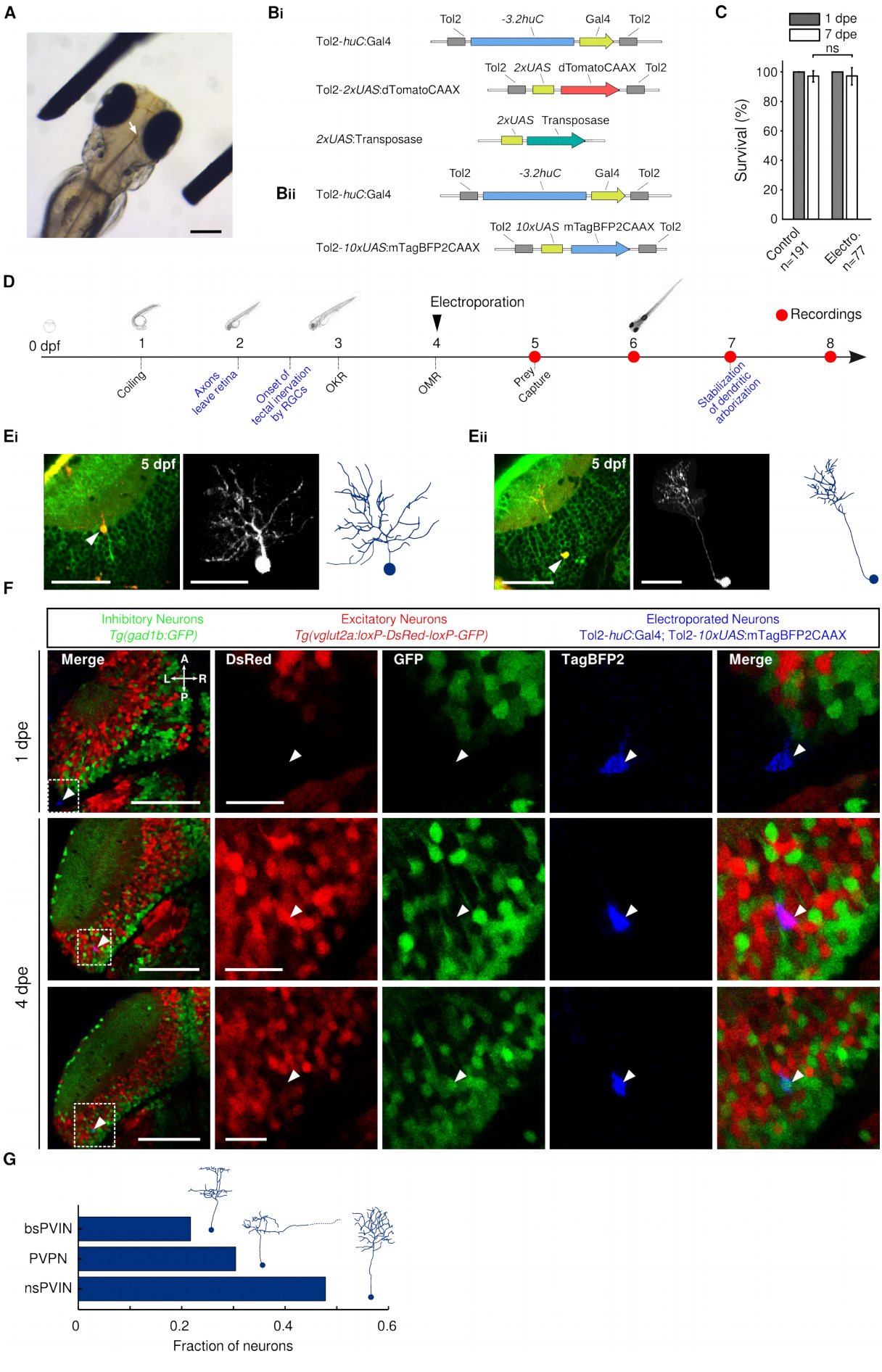
A
Bi
Tol2
-3.2huC
Gal4
Tol2
Tol2-huC:Gal4
Tol2 2xUAS dTomatoCAAX Tol2
Tol2-2xUAS:dTomatoCAAX
2xUAS Transposase
2xUAS:Transposase
Bii
Tol2-huC:Gal4
Tol2 10xUAS mTagBFP2CAAX Tol2
Tol2-10xUAS:mTagBFP2CAAX
C
1 dpe
7 dpe
ns
Survival (%)
100
80
60
40
20
0
Control n=191
Electro. n=77
D
Electroporation
Recordings
0 dpf
1
2
3
4
5
6
7
8
Coiling
Axons leave retina
Onset of tectal inervation by RGCs
OKR
OMR
Prey Capture
Stabilization of dendritic arborization
Ei
5 dpf
Eii
5 dpf
F
Inhibitory Neurons
Tg(gad1b:GFP)
Excitatory Neurons
Tg(vglut2a:loxP-DsRed-loxP-GFP)
Electroporated Neurons
Tol2-huC:Gal4; Tol2-10xUAS:mTagBFP2CAAX
Merge
A
L
R
P
DsRed
GFP
TagBFP2
Merge
1 dpe
4 dpe
G
bsPVIN
PVPN
nsPVIN
0
0.2
0.4
0.6
Fraction of neurons

***Figure S1 related to Figure 1*. Morphological development and emergence of neurotransmitter identity of newborn neurons**

(A) Picture of the electroporation preparation with the electrodes positioned on both sides of the larva. White arrow: the capillary containing DNA introduced in the tectal ventricle. Scale bar: 200 µm.

(B) i, DNA constructs used for labeling newborn neurons in *Tg(huC:GCaMP5G).* Long-term expression of the vectors was achieved using the co-electroporation of a transposase enabling the stable incorporation of the constructs flanked with Tol2 sites, into the larva's genome. **ii**; Constructs used for labeling newborn neurons in *Tg(gad1b:GFP;vglut2a:loxP-DsRed-loxP-GFP)*.

(C) Quantification of the survival of electroporated larvae and age-matched controls, at 1 and 7 dpe. Note that electroporations did not show any significant effect in the survival of the larvae. ns.: $p > 0.05$.

(D) Time-course of the zebrafish larva development from 0 to 8 dpf, in terms of morphology, behavior and maturation of the visual system. Performing electroporations at 4 dpf enables studying the development of newborn neurons as they incorporate into an already functionally mature brain structure. OKR: optokinetic response and OMR: opto-motor response. Red dots: the developmental stages at which we performed the experiments. Arrow-head: the developmental stage at which we performed the electroporations.

(E) Two examples of mature neurons in 5 dpf larvae (**i** and **ii**). Left**,** position of the soma of the labeled neuron (arrow-head), within the PVZ layer of the optic tectum. Scale bar: 50 µm. Middle, a 3D projection of the mature neuron showing the neuron's morphology. Scale bar: 20 µm. Right, reconstruction of the neuron in the middle panel. Note that in contrast to the newborn-labeled neurons at 5 dpf (1 dpe), neurons far from the neurogenesis site already show mature morphologies. The neurons were labeled using single-cell electroporation in *Tg(huC:GCaMP5)* larvae.

(F) Examples of *Tg(gad1b:GFP;vglut2a:loxP-DsRed-loxP-GFP)* larvae electroporated with Tol2-*huC*:Gal4 and Tol2-*10xUAS*:mTagBFP2CAAX constructs. Electroporated newborn neurons are indicated with white arrow-heads. Top, a newborn neuron not yet differentiated at 1 dpe. Middle and bottom, differentiated excitatory and inhibitory neurons at 4 dpe. First column: optical plane of

the optic tectum showing inhibitory (green), excitatory (red) neurons and a single newborn neuron (blue and arrow-head). Scale bars: 20 µm. Second, third and fourth columns, zoom of the dashed region in the first column, for the red, green and blue channels, respectively. Fifth column, all channels merged. Scale bars: 50 µm. L: left, R: right, A: anterior and P: posterior.

(G) Based on the morphology of the dendritic arbors at 4 dpe, newborn-labeled neurons developed into different neuronal types. Fraction of the different neuronal types. nsPVIN: non-stratified periventricular interneurons. PVPN: periventricular projection neurons. bsPVIN : bi-stratified periventricular interneurons.

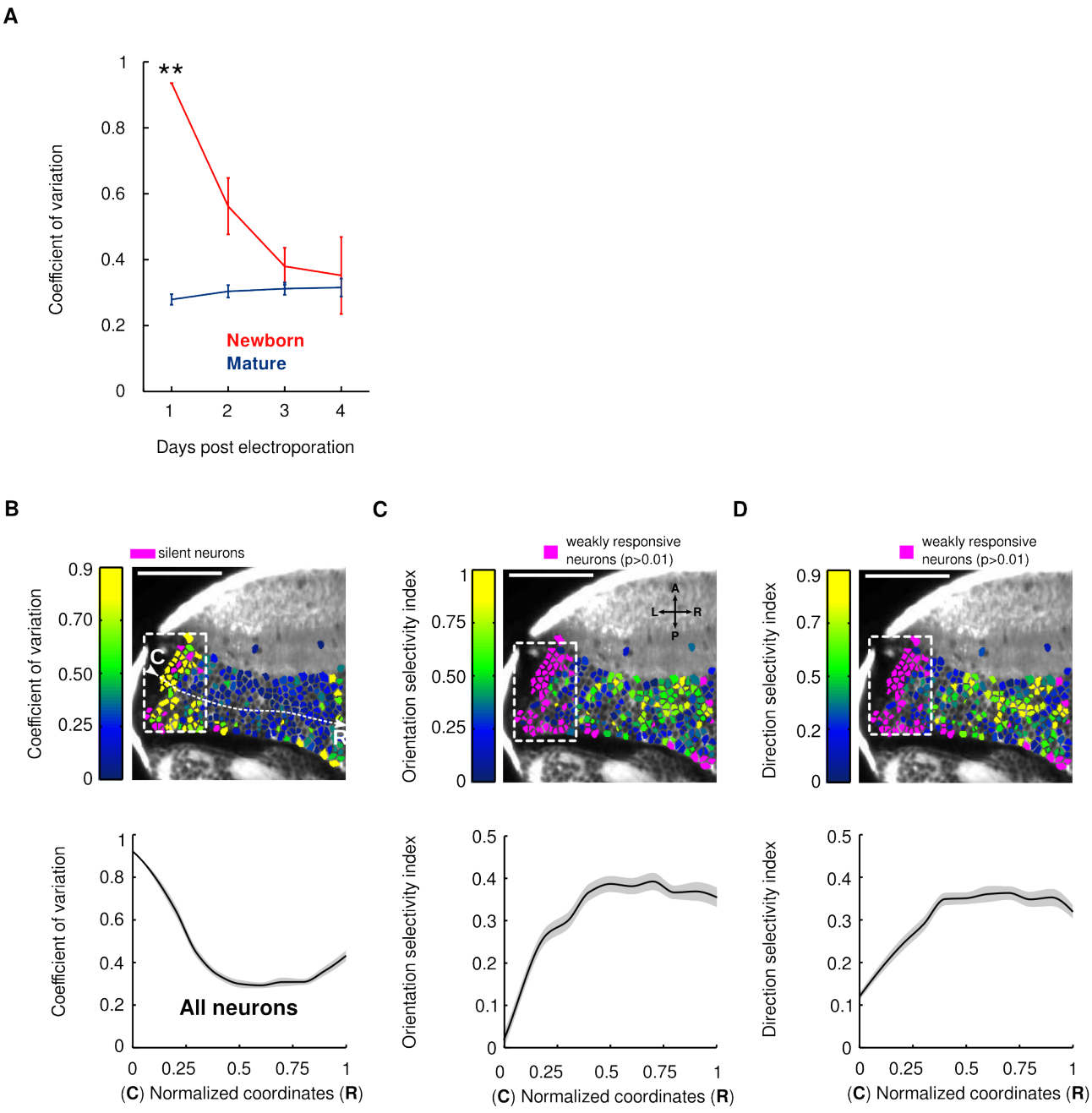

Figure S2 related to Figure 2. **Development of functional intrinsic and visually induced properties of newborn neurons**

(A) Development dynamics of the coefficient of variation of neuronal responses to drifting gratings, for newborn-labeled (red) and mature (blue) neurons (newborn-labeled neurons: n=7, 10, 6 and 3, for 1-4 dpe, respectively; mature neurons: n=973, 1340, 858 and 453 mature neurons, from 5, 7, 4 and 2 larvae). **: $p < 0.01$. Error bars: SEM

(B-D) Top, example of an optical plane of the optic tectum with neurons color-coded according to

their coefficient of variation (B), orientation (C) and direction-selectivity index (D). Magenta: poorly responsive neurons (in C-D, $p>0.01$, Mann-Whitney U tests or silent neurons in B). Note that these neurons were mainly clustered in close vicinity of the neurogenesis region (dashed area). Neurons with noisy baseline were left unlabeled. Arrows: orientation of the larva: L: left, R: right, A: anterior and P: posterior. Scale bar: 50 µm. Bottom, averaged distributions of the measured parameters on top, across the normalized coordinates along the caudo-rostral axis (white dashed curve on top, C: caudal, R: rostral), for all neurons, from 5 to 8 dpf (n=5046 neurons, from 18 larvae). Confidence interval: SEM. Changes in the orientation-, direction-selectivity index and coefficient of variation were significant across the caudo-rostral axis ($p=7.61x10^{-20}$, $p=4.29x10^{-23}$ and $p=4.57x10^{-33}$, respectively, Kruskal-Wallis tests). Note the large differences for the three measured parameters close to the neurogenesis region (dashed region). Neurons involving few pixels (less than 5) or with unstable baselines (rapid changes generally indicating movement artifacts) were left unlabeled.

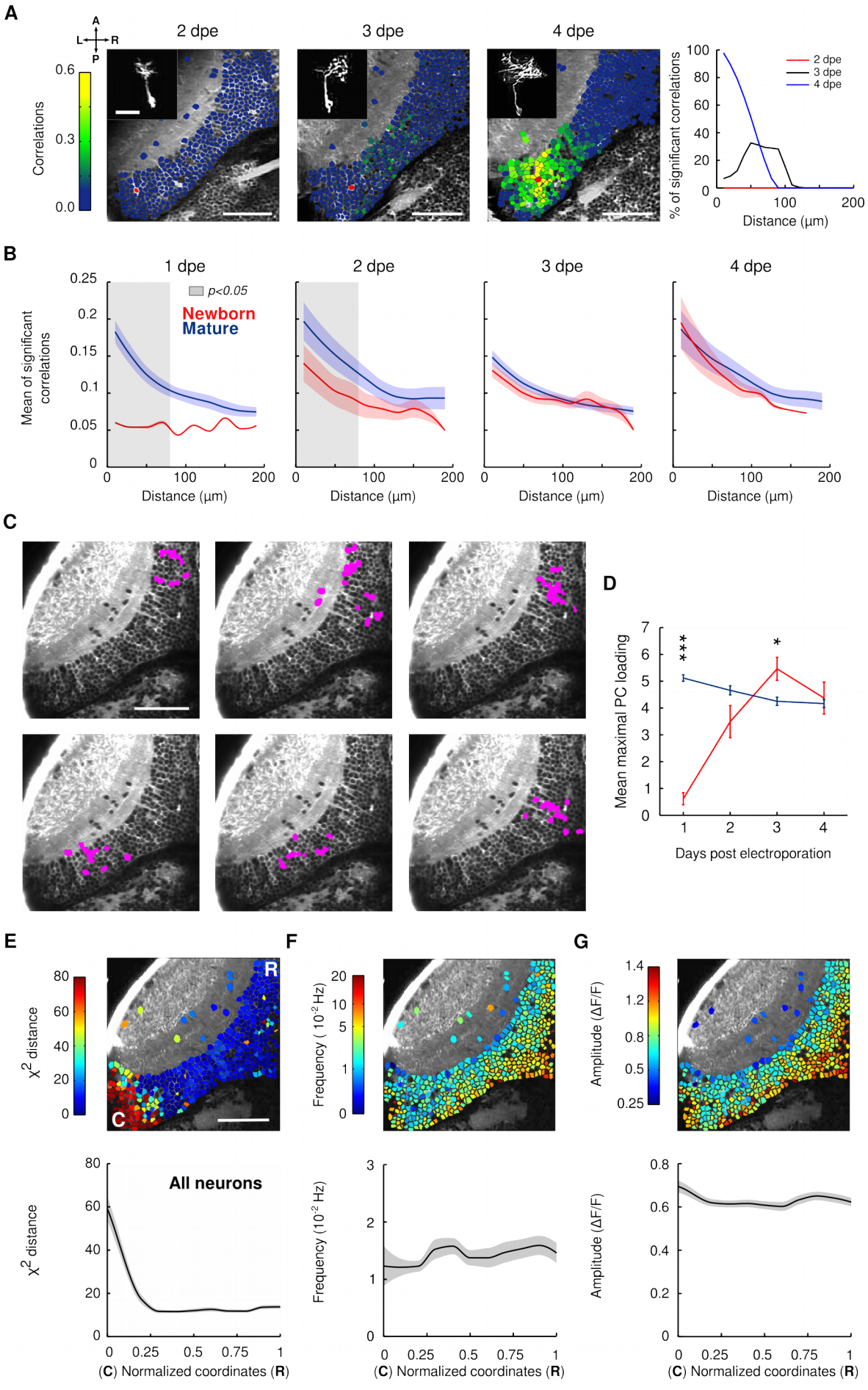
A
2 dpe
3 dpe
4 dpe
Correlations
% of significant correlations
Distance (µm)
B
1 dpe
2 dpe
3 dpe
4 dpe
p<0.05
Newborn
Mature
Mean of significant correlations
Distance (µm)
C
D
Mean maximal PC loading
Days post electroporation
E
F
G
χ2 distance
Frequency (10-2 Hz)
Amplitude (ΔF/F)
All neurons
(C) Normalized coordinates (R)

***Figure S3 related to Figure 5*. Spontaneous activity correlations between newborn-labeled and mature tectal neurons**

(A) Left, example of an optical plane of the optic tectum containing a newborn-labeled neuron (red) chronically imaged from 2 to 4 dpe. Neurons are color-coded according to their pair-wise correlation values with the newborn-labeled neuron. Color scale bar: Pair-wise correlations between the newborn-labeled neuron and the rest of the tectal neurons. Scale bars: 50 µm. Insets: Morphology of the newborn-labeled neuron. Scale bars: 20 µm. Right, the percentage of significant correlations between the developing newborn-labeled neurons and the rest of the tectal cells, with respect to the physical distance between the neurons, for 2 (red), 3 (black) and 4 (blue) dpe. Neurons involving few pixels (less than 5) or with unstable baselines (rapid changes generally indicating movement artifacts) were left unlabeled.

(B) The developmental dynamics of the relationship between the mean of significant correlations and the physical distance between the neurons, for the newborn-labeled neurons (red) and the mature neurons (blue), from 1 to 4 dpe. Confidence intervals: SEM. Gray shaded areas: significant differences between newborn and mature curves ($p<0.05$, Mann-Whitney U tests).

(C) Examples of 6 spontaneous neuronal assemblies showing their topographies. Magenta: neurons within an assembly.

(D) The maximal principal component loadings for newborn-labeled and mature neurons. Maximal principal component loadings reflect the level of prediction of the activity of a neuron by the activity of the assembly which contains it, assuming that each neuron belongs only to one assembly. *: $p<0.05$. ***: $p<0.001$. Error bars: S.E.M, newborn neurons: n= 6, 15, 21, 15; mature neurons: n=1962, 3564, 5296, 3969, from 6, 10, 17 and 11 larvae, respectively.

(E-G) Top, example of an optical section of the optic tectum showing neurons color-coded according to X^2 distance (high values indicate low level of significant correlations), the frequency of the spontaneous Ca^{2+} events (middle), and the amplitude of the spontaneous Ca^{2+} events (right). The X^2 distance is the euclidean distance between the average distribution represented in **Figure 5**C (mature neurons, blue curve) and the distribution of each neuron, for distances shorter than 60µm. High X^2 values indicate neurons that are isolated from others (do not show significant correlations with other neurons). Bottom, averaged distributions of the measured parameters, across the

normalized coordinates along the caudo-rostral axis, for all neurons, from 5 to 8 dpf (n=17678 neurons, from 44 larvae). Confidence interval: SEM. Changes in the X^2 distance across the caudo-rostral axis were significant, while the frequency and amplitude of the spontaneous Ca^{2+} events did not show significant changes ($p=4.12x10^{-6}$, p=0.55 and p=0.26, respectively, Kruskal-Wallis tests). Neurons involving few pixels (< 5) or with unstable baselines (rapid changes generally indicating movement artifacts) were left unlabeled.

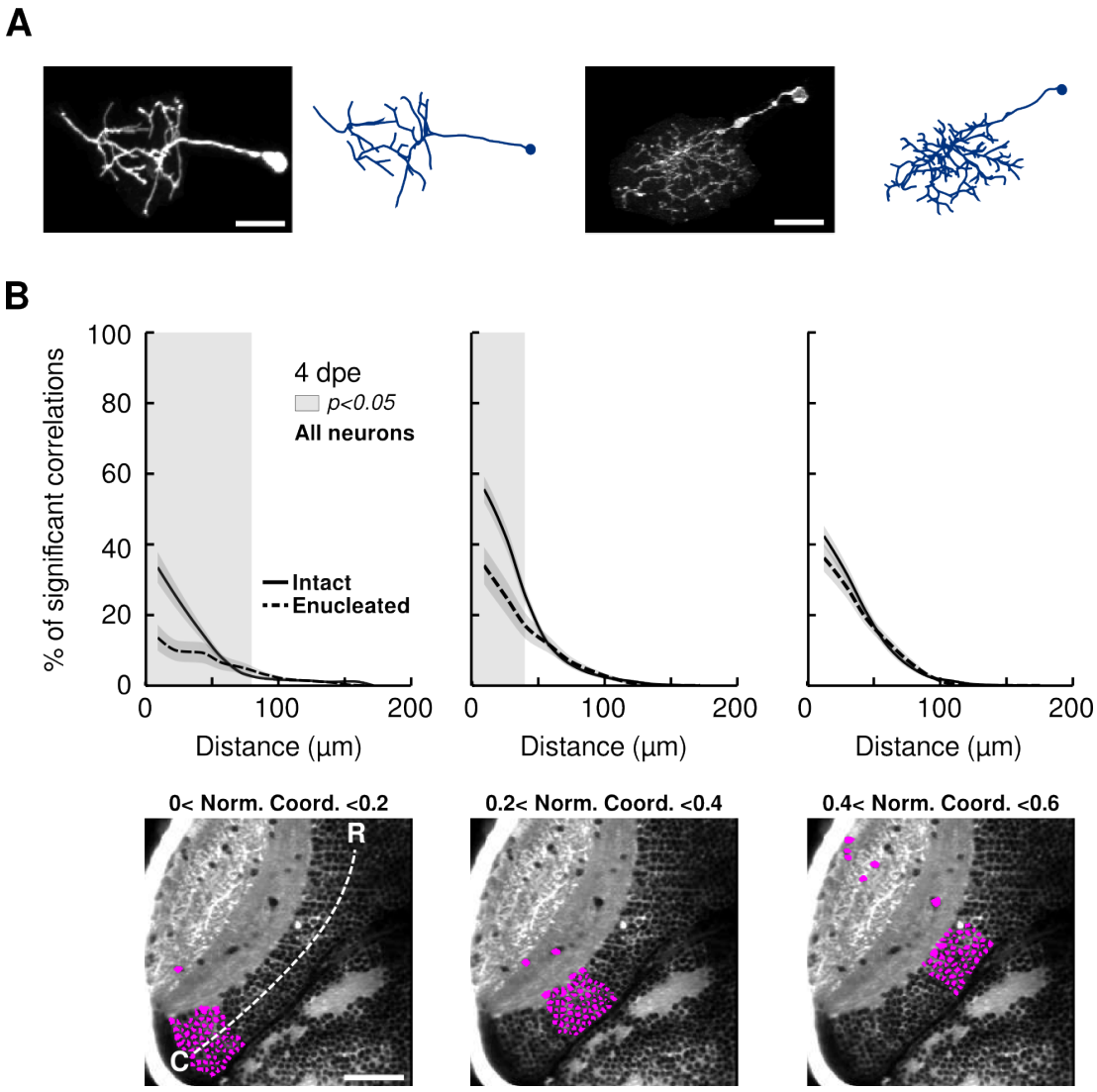

***Figure S4 related to Figure 6*. Enucleations prevent neurons from newborn neurons from incorporation into the mature tectal circuit but do not affect the development of their morphology.**

(A) Two examples of the morphology of newborn-labeled neurons at 4 dpe after when enucleations were performed at 3.5 dpf. Left, a projection of the newborn-labeled neuron showing the developed dendritic morphology. Scale bar: 20 µm. Right, reconstruction of the neuron on the left.

(B) Top, the percentage of significant correlations with respect to the distance between neurons, at three different regions of the optic tectum (caudal, medial and rostral along the caudo-rostral tectal axis), at 4 dpe, for intact (solid line) and enucleated (dashed line) larvae. Bottom, an example of an optical section of the optic tectum showing the neurons (magenta) belonging to the three tectal regions (caudal: 0-0.2, medial 0.2-0.4, rostral: 0.4.0.6) used for the analyses in the top panel.

	Functionally mature neurons	Newborn-labeled neurons	Functionally immature neurons
1 dpe	161.7±19.4	37.9±22.6	138.8±24.3
2 dpe	353.7±61.7	72.0±11.9	309.9±61.6
3 dpe	194.0±29.0	159.6±78.2	175.6±30.2
4 dpe	157.6±7.6	65.7±20.8	149.4±11.0
Enucleated 4 dpe	106.3±9.1	55.2±15.2	92.6±8.5

***Table S1 related to Figure 4 and 6*.** **Number of significant spontaneous Ca^{2+} events for all experimental conditions.** The average number of significant Ca^{2+} events during one-hour recordings and the standard error, for all experimental conditions (1 to 4 dpe in normal and enucleated larvae), for mature, newborn-labeled, and immature neurons. The difference in the number of events between the newborn-labeled and the functionally immature neurons partially contradicts **Figure S3**F. This difference could be explained by the fact that dTomato expression impeded the detection of low-magnitude Ca^{2+} events (due to quenching and/or cross talk between channels).